Summer 8-12-2014

Optimization of Thiolate Stabilized Gold Nanoclusters For Near Infrared Emission in Subcellular Imaging

Cecil Vincent Conroy
Georgia State University, cconroy4@student.gsu.edu

OPTIMIZATION OF THIOLATE STABILIZED GOLD NANOCLUSTERS FOR NEAR INFRARED EMISSION IN SUBCELLULAR IMAGING

by

CECIL VINCENT CONROY

Under the Direction of Dr. Gangli Wang

ABSTRACT

Monothiolate protected gold nanoclusters with near IR luminescence underwent a five-to-ten fold enhancement of quantum efficiency by heating in the presence of excess thiols. Two monothiolate nanoclusters, mercaptosuccinic acid and tiopronin, were shown to benefit from this procedure. Emission maximum around 700-900 nm is favorable for bioimaging applications due to reduction of background signal from autofluorescence. Dithiolate lipoic acid protected gold nanoclusters with higher near IR quantum efficiency present an interesting candidate for biological imaging due to the difference in hydrophobicity, resistance to quenching by divalent cations and cell growth media, and retained quantum efficiency when coupled to agents such as polyethylene glycol. Intracellular and nuclear internalization of mercaptosuccinic gold nanoclusters demonstrate a potential vector for delivery of nuclear targeting agents. The small size, chemical stability, high luminescence, and potential for targeting various intracellular domains make gold nanoclusters worthwhile for further studies as potential bioimaging probes.

INDEX WORDS: Gold nanoclusters, Thiol, Near-IR luminescence, Confocal imaging

OPTIMIZATION OF THIOLATE STABILIZED GOLD NANOCLUSTERS FOR NEAR INFRARED EMISSION IN SUBCELLULAR IMAGING

by

CECIL VINCENT CONROY

A Thesis Submitted in Partial Fulfillment of the Requirements for the Degree of

Master of Science

in the College of Arts and Sciences

Georgia State University

2014

OPTIMIZATION OF THIOLATE STABILIZED GOLD NANOCLUSTERS FOR NEAR INFRARED EMISSION IN SUBCELLULAR IMAGING

by

CECIL VINCENT CONROY

Committee Chair: Gangli Wang

Committee: Suri S. Iyer

Jun Yin

Electronic Version Approved:

Office of Graduate Studies

College of Arts and Sciences

Georgia State University

August 2014

DEDICATION

I would like to thank my mother, Vicky Howard, and father, Vincent P. Conroy, for their love and support. I also thank my brothers Evan and Collin for everything they have done.

ACKNOWLEDGEMENTS

I would like to thank Dr. Gangli Wang for letting me work under his guidance and for all of the support and advice. I also thank past and present colleagues Dr. Zhenghua Tang, Dr. Tarushee Ahuja, and Dr. Jie Jiang for their help in not only training but also for feedback over time. I thank Dr. Chen Zhang for her willingness and flexibility in our collaboration with cell imaging studies. I thank Sisi Jiang of Dr. Peng George Wang's lab for the opportunity to try working with some carbohydrates. I would like to thank Jonathan W. Padelford, amongst other reasons, for helping me to run some of the experiments leading to the creation of this thesis. I thank Dr. Zhenming Du and Dr. Bin Xu for their assistance with NMR. Dr. Jeremiah D. Harden, Dr. Gigi B. Ray, and many other GSU faculty I thank for their advice and encouragement to pursue advanced study in the field of chemistry. I appreciate the opportunities provided by Dr. Dabney W. Dixon and Dr. Susanna F. Greer for the opportunity to look at investigating a new teaching lab experiment and the GSU summer undergraduate Molecular Basis of Disease fellowship, respectively. Last, but not least, I would like to thank every member of the Gangli Wang research group for everything that comes along with working as a team during my stay with the lab.

TABLE OF CONTENTS

LIST OF TABLES

LIST OF FIGURES

LIST OF ABBREVIATIONS

AIE	aggregation-induced emission
Au NCs	gold nanoclusters
Au NPs	gold nanoparticles
CHCA	α-cyano-4-hydroxycinnamic acid
DAPI	4',6-diamidino-2-phenylindole
DMPS	2,3-dimercaptopropanesulfonate
DOS	density of states
DTTC	3,3'-diethylthiatricarbocyanine iodide
Durene-DT	4,5-bis(mercaptomethyl)-o-xylene
EDC	N-(3-dimethylaminopropyl)-*N'*-ethylcarbodiimide hydrochloride
ESI	electrospray ionization
HEK293	human embryonic kidney 293 cells
HeLa	HeLa human cervical cancer cells
InGaAs	indium gallium arsenide
kDa	kilo Dalton
LA	lipoic acid
m/z	mass over charge
MALDI	matrix-assisted laser desorption ionization
MS	mass spectrometry
MSA	mercaptosuccinic acid
MTT	methyl thiazolyl tetrazolium
MUDA	11-mercaptoundecanonic acid
NLS	nuclear localization signal
NMR	nuclear magnetic resonance
NPs	nanoparticles
PAMAM	polyamidoamine
PBS	phosphate buffered solution
PEG	methoxypolyethylene glycol
PhC2S	phenylethanethiolate
PMT	photomultiplier tube
ppm	parts per million
QE	quantum efficiency
Rh	rhamnose-propyl amine
Au(SG)	gold glutathione
THAM	tris(hydroxymethyl)aminomethane
Tio	tiopronin (N-(2-mercaptopropionyl)glycine)
UV	ultraviolet
Vis	visible

1 INTRODUCTION

1.1 Gold nanoclusters

Gold nanoparticles (Au NPs) are of fundamental interest as an intermediate between the chemical properties of bulk gold and atomic gold. These properties have led to research aimed at taking advantage of them for use in biomedical applications.[1] Bulk gold has very low luminescence while Au NPs have quantum efficiencies that are higher by several orders of magnitude.[2] A frequently used synthetic technique is the Brust-Schiffrin synthesis.[3] Au NPs are synthesized by using a thiol ligand to stabilize small groupings of gold atoms to prevent gold aggregation to the point of behavior approaching that of bulk gold. The strong gold-sulfur bond is the basis of many synthesized Au NPs. As an example of another synthesis technique, another method has been to use dendrimers, e.g. polyamidoamine (PAMAM). PAMAM is initially used to form small clusters of gold atoms that subsequently undergo ligand exchange with the thiol of choice.[4]

One interesting characteristic of larger gold nanoparticles is a surface plasmon. For spherical gold nanoparticles this can be observed as a peak in the absorbance spectrum at approximately 520 nm. When the gold nanoparticles absorb this wavelength of light, they quickly heat up leading to local areas of intense heat. Research into this as a possible targeted anti-cancer treatment has shown it may be feasible future method of treatment.[5]

A subgroup of gold nanoparticles are the gold nanoclusters (Au NCs). They border the region between atomic gold and the larger Au NPs, but in this case a defined composition is obtainable. An energy gap between the highest occupied molecular orbital (HOMO) and lowest unoccupied molecular orbital (LUMO) of sufficient magnitude to lead to luminescence upon energy relaxation is required for intrinsic fluorescence. Unequal energy between the emission energy

and the band gap energy have been shown for Au NCs.[6,7] The large difference in energy between excitation and emission wavelengths suggests significant energy relaxation is occurring.[8] This has been shown for Au NCs with a core diameter smaller than 2.2 nm.[9,10] The interaction between gold and sulfur atomic orbitals is thus of much interest in the pursuit of enhancing the optical properties of Au NCs. Emission wavelength can be tailored by changing the core size and ligand.[11,12,13] Accompanying the transition to smaller sized Au NCs is the emergence of absorption peaks that correspond with specific size gold cores such as $Au_{22}(SR)_{18}$, $Au_{25}(SR)_{18}$, $Au_{38}(SR)_{24}$, $Au_{102}(SR)_{44}$.[6]

1.1.1 Core-ligand structural studies

This core-ligand interface is of such importance to the properties of Au NCs that it only makes sense that research has been put forth to determine the structural arrangement at the interface. It was shown that there is not a simple Au-S structure, but rather there are arrangements such as S-Au-S and S-Au-S-Au-S, found in $Au_{102}(SR)_{44}$ and $Au_{25}(SR)_{18,}$ that are now referred to as the staple motif.[14,15] This can be seen in Figure 1 when only the Au core and ligand sulfur atoms are displayed. In Figure 1B the thirteen atom gold core can clearly be seen surrounded by multiple staple motif structures. The $Au_{102}(SR)_{44}$ structure was determined with para-mercaptobenzoic acid as ligand, while other Au NCs structures have been studied with other ligands. Crystallization of $Au_{25}(SCH_2CH_2Ph)_{18}$ made possible structural studies. Crystallization of $[TOA^+][Au_{25}(SCH_2CH_2Ph)_{18}^-]$ revealed a distorted ligand arrangement around the gold core that made room for the stabilizing cation.[15] Further examination of both the anionic and neutral $Au_{25}(SCH_2CH_2Ph)_{18}$ demonstrated the neutral species did not display the distorted ligand arrangement of the anionic species. Additionally, the optical properties varied with absorption peaks varying in strength and broadness while maintaining their general location.[16,17]

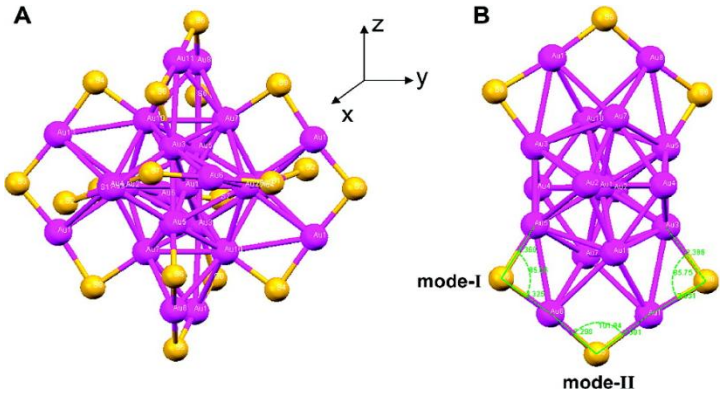

Figure 1. Structure of $Au_{25}(SR)_{18}$ nanocluster. Reprinted with permission from Wu, Z.; Gayathri, C.; Gil, R. R.; Jin, R., *J. Am. Chem. Soc.* 2009, *131*, 6535. Copyright 2009 American Chemical Society.

That begged the question of how different thiolate ligands affect the structure. $Au_{25}(SG)_{18}$ NCs have been studied by multiple groups owing in part to good stability, but crystallization for structural analysis proved more difficult. NMR, mass spectrometry, and optical measurements were used to get around this hurdle. Mass spectrometry was used to compare the fragmentation patterns between $Au_{25}(SCH_2CH_2Ph)_{18}$ and $Au_{25}(SG)_{18}$. Comparison of the two mass spectra showed comparable results. 1D and 2D NMR analysis revealed splitting of the α-CH_2 and β – CH. The authors commented that those hydrogen atoms nearest the gold core would be more sensitive to the redox state of the core. Thus analysis of the splitting demonstrated a 2:1 ratio between glutathione bound to the Au_{13} core atoms versus glutathione bound to the Au_{12} shell atoms. This observation was in agreement with the findings for $Au_{25}(SCH_2CH_2Ph)_{18}$. Additionally, the optical absorption spectrum of $Au_{25}(SG)_{18}$ matched that of anionic $Au_{25}(SCH_2CH_2Ph)_{18}$. It was concluded the structure of both Au_{25} NCs were comparable.[18]

1.1.2 Quantum efficiency vs. ligand polarity

The aforementioned potential for different ligands to affect Au NCs properties has been observed on the quantum efficiency (QE) of Au NCs. Ligand exchange of nonpolar

hexanethiolate Au_{140} NCs with (N,N,N-trimethyl-(mercaptoundecyl)ammonium), which has a positive charge, resulted in a linear increase in emission intensity with increasing average number of positively charged ligands on the Au_{140} core. Additional work studying both Au_{38} and Au_{140} core NCs demonstrated establishing more charge, or even just more polar functional groups, led to an increase in emission intensity. $Au_{38}(SC_2H_4Ph)_{24}$ underwent ligand exchange with more polar thiols including 4-chlorothiophenol, tiopronin, and 2-mercaptoethanol. The resulting ligand exchange reactions increased the emission intensity with some species also showing a change in emission wavelength.[13]

Keeping in mind the previously discussed changes in structure based on core charge, an investigation into the effect of core charge on emission intensity involved bulk electrolysis of $Au_{140}(S(CH_2)_5CH_3)_{53}$. The uncharged NCs exhibited no emission, but upon bulk electrolysis to oxidize the core the intensity increased. Further investigation showed the emission intensity increased more so with a longer alkane thiol, C12 versus C5 or C6, for oxidized versus neutral NCs. This was explained by the longer nonpolar ligand better screening the charged core from the effect of solvent or supporting electrolyte. The result was to enhance the polarization of the Au-S bond further toward sulfur.[13] Additionally, the core-ligand charge interaction is another possible effect to take into consideration.[19]

Research has not yet led to a predictive model between the method of synthesis and particle size and emission wavelength and Q of Au NCs. Zheng *et al.* provided a good summary of gold nanoclusters and nanoparticles luminescence and the different models used to describe the properties of previously synthesized particles.[20] A summary of some of the particles discussed in the review and elsewhere, as shown in Table 1, shows the role core size and ligand play on emission maximum and quantum efficiency. Note the table is only a modest selection of a broader

range of gold nanoclusters, but it demonstrates the fluctuations in both emission maximum based on both core size and ligand structure.

Table 1. Comparison of some known gold core sizes and ligand structures to reported emission maximum.

Au NCs composition	**Emission maximum (nm)**	**Quantum efficiency**	**Ligand**	**Solvent**
Au5	385	7×10^{-1}	poly(amidoamine)[11]	aqueous
Au8	455 505 465	4×10^{-1} $1\text{-}2 \times 10^{-1}$ 0.15	poly(amidoamine)[11] polyethylenimine[21] etched with glutathione[22]	aqueous
Au13	510	2.5×10^{-1}	poly(amidoamine)[11]	aqueous
Au15(SR)13	425 825	1×10^{-3} 2×10^{-4}	glutathione[23]	aqueous
Au22(SR)16	775	4×10^{-3}	glutathione[23]	aqueous
Au22(SR)17	730	2×10^{-3}	glutathione[23]	aqueous
Au23	760	1.5×10^{-1}	poly(amidoamine)[11]	aqueous
Au25(SR)18	825	1×10^{-3}	glutathione[23]	aqueous
Au25(SR)18	640	6×10^{-2}	bovine serum albumin[24]	aqueous
Au25(SR)18	500 710	Not stated Not stated	glutathione[25]	aqueous
Au25(SR)18	500 ~900	10^{-6} to 10^{-7} Not stated	C6[25]	dichloromethane
Au28(SR)16	840, 1080	1.5×10^{-3} 2.0×10^{-3}	glutathione[8]	aqueous
Au29(SR)20	885	3×10^{-7}	glutathione[23]	aqueous
Au31	866	10^{-1}	poly(amidoamine)[11]	aqueous

1.1.3 Core and surface-ligand modification

Research has also been directed into tailoring existing NCs to better suit the requirements of potential applications. One approach has been to take larger Au NPs and heat them in the presence of excess free thiol. The process is not well understood, but is hypothesized to take one of two routes. The first route is the free thiol etches away gold atoms from the core, reducing the

size of the nanoparticle. The second route is the Au(I)-thiolates pulled off the nanoparticle then form smaller clusters due to interaction of their occupied and unoccupied orbitals.[22] Multiple groups have investigated the etching technique.[22,26,27] One investigation used laser desorption mass spectrometry, absorbance, and X-ray diffraction to observe 14 kDa NCs getting focused down to 8 kDa NCs.[26] Another group used Au-mercaptosuccinic acid NCs (Au-MSA NCs) as the starting product. Adjusting the pH to 3 prior to etching with excess glutathione resulted in Au_{25} core. However, a pH of 8 led to Au_8 core despite starting from the same starting NCs.[22]

Annealing is another process that has been used to improve Au NPs characteristics. This process is similar to etching, but the temperature is much more moderate and the ratio of free thiols to Au NPs is much lower. Rather than etching away the gold core, the annealing process focuses on optimizing the core-ligand interface. It is also possible the annealing process results in the elimination of Au NPs with less favorable thermodynamic stability. It has been shown to improve the resolution of the electrochemical measurements of hexanethiolate stabilized gold nanoclusters.[28]

1.1.4 Ligand addition and exchange

Thus far monothiolate ligands have been discussed to stabilize the gold core, but dithiolate ligands have also been studied with some very interesting observations. There is also the question of what happens when a dithiol is introduced into solution with monothiolate protected Au NCs or vice versa. Entropy would suggest the dithiol would displace the monothiolates. The more sterically hindered structure of a dithiol, however, may not lead to the same combination of Au and S atomic orbitals. How does that affect the optical and chemical properties of the Au NCs? Does changing the length of the carbon chain that serves as the back-

bone for the ligand affect the properties? Do both sulfur atoms remain bonded to the core, or does the steric strain lead to the breaking of one core-ligand bond?

Ligand exchange between monothiol tiopronin and dithiol 2,3-dimercaptopropanesulfonate (DMPS) were investigated by addition of one type thiol to Au NCs stabilized by the other type thiol. The addition of DMPS to Au-Tio NCs resulted in a decrease in emission intensity over time. The absorption spectrum showed a slowly increasing peak at 282 nm. This peak corresponds to Au_4-DMPS clusters and suggested more had occurred than a simple ligand exchange. The change in absorbance continued over the span of three weeks, but the change in emission intensity stabilized over a span of days. A two-step process was proposed where initially ligand exchange was taking place. The second step was the slow etching of the Au core to form Au_4-DMPS that was also observed in MALDI MS.[29]

Approaching from the opposite direction, the addition of tiopronin to Au-DMPS NCs demonstrated a different trend. Where initially Au-DMPS NCs were not luminescent, emission intensity increased over time with exposure to free tiopronin. The absorbance peak at 282 nm also increased a little, suggesting the formation of Au_4-DMPS. However, free Au_4-DMPS was not detected by ^{1}H NMR. Tiopronin peaks were broadened in the ^{1}H NMR spectrum. Taken together, this suggests tiopronin had been added to the Au core rather than undergoing an exchange reaction with DMPS. MALDI MS data revealed more fragmentation than observed with the addition of DMSP to Au-Tio NCs. The intensity of Au_4DMPS_3 was higher than Au_4DMPS_4, which suggested surface rearrangement rather than an etching process.[30]

An investigation looking at the phenylethanethiolate (PhC2S) and 1,4-dithiolate durene Au NCs demonstrated a different effect from what was found with tiopronin and DMPS. The addition of durene-DT to PhC2S Au NCs resulted in the loss of distinct peaks in the absorption

spectrum while emission intensity increased over time. This change in the absorption spectrum suggests a change in the Au core. The addition of durene-DT to the core was supported by ^{1}H NMR that showed the line broadening effect occurring over time for the CH_3 and CH_2 peaks. The opposite effect, sharpening of the CH_2 peaks, was observed for the PhC2S as it became unbound to the gold core showing it exchanged with Durene-DT.

Approaching it from the opposite direction, the addition of PhC2SH to durene-DT Au NCs resulted in a decrease in emission intensity over time. Specific absorption peaks in the spectrum did not match those of the PhC2S stabilized Au NCs, but initial synthesis with two different ligands would not necessarily produce Au cores of the same size. The lack of change in the absorption spectrum suggested little changed with the Au core relative to the previously discussed loss of absorbance peaks. The ^{1}H NMR spectrum showed the opposite line broadening effect trends as one would expect given the reversal in ligand exchange direction. This was different from the previous system in that the monothiol PhC2S displaced durene-DT while the monothiol tiopronin was added to the Au core through surface rearrangement.[29] The different responses in emission intensity and addition versus exchange when looking at 1,2 versus 1,4 dithiols begs the question of what would occur with other monothiolate and dithiolate systems.

1.2 In vitro Au NCs cell imaging

The many conjugated bonds present in biomolecules, such as in the amino acid tryptophan, lead to autofluorescence of biological solutions. The span of autofluorescence is from the near UV through the visible region (~250-650 nm). Any fluorescent dye intended for biological application thus has to contend with this autofluorescence by either having a strong enough emission to pierce through the background emission or emit outside this region. The latter approach, minimizing the interference of extraneous emission, can put to use the large energy re-

laxation characteristic of Au NCs. While many dyes have a Stokes shift of less than 100 nm, Au NCs have been demonstrated to have Stokes shifts of 300-400 nm. Such a large energy relaxation also facilitates the use of a longpass filter to cut down on autofluorescence intensity reaching the detector.

Research has been progressing on what happens when Au NCs and NPs are added to biological systems ranging from cell incubation studies to animal scale experiments. Au NCs stabilized by 11-mercaptoundecanoic acid (MUDA) were used to study the possibility to target the nuclear region. A nuclear localization signal (NLS), the peptide SV40, was coupled to the ligands. Confocal fluorescent imaging of HeLa cells demonstrated entry of the gold NCs into the nucleus while the same particles, without coupled NLS were unable to enter either the nucleus or cell.[31] Targeting of human hepatoma cells (HepG2) by streptavidin coupled Au_{23} NCs was shown effective with confocal fluorescence imaging. The same Au_{23} NCs, but without the coupling of streptavidin, were not observed to target HepG2 cells. Streptavidin was used as a targeting agent due to the high affinity for biotin present on HepG2 cells.[32]

The complexity of biological systems necessitates considering factors that were previously not a consideration when working with much more defined solutions, e.g. ultrapure water or analytical grade solvents. A charged ligand dissolved in cell growth media will attract various biomolecules. Accumulation of biomolecules around Au NCs leads to the formation of a protein corona.[33] This protein corona changes how the NCs interact with the cell membrane because the ligand functional groups are no longer what interact with cell membrane.

Will divalent cations, e.g. Ca^{2+}, lead to crosslinking and aggregation of NCs with anion containing ligands? Addition of various cations, mostly divalent cations, was tested with Au-

glutathione NCs. In that report, only Cu^{2+} ions had a significant effect on emission intensity, immediately quenching nanoclusters emission.[32]

Nanocluster concentration has also been shown to play a role in cellular uptake. Some small Au NCs were shown to have a linear relationship between concentration and rate of entry into cells up to a certain level after which the rate plateaus. Multiple smaller Au-lipoic acid NCs (Au-LA NCs) were required to adhere to HeLa cell membrane before endocytosis was triggered. A linear trend was observed for 2-20 μg/mL with higher concentrations, 40-80 μg/mL, showing a leveling off of rate of uptake. The kinetics of Au-LA NCs were observed to increase over the first hour while reaching a plateau around the two hour mark.[34] The requirement for multiple small particles to first adhere to the membrane prior internalization had previously been observed for nanoparticles.

The photoluminescence characteristics would be of little use if the nanoclusters proved to be toxic to cells, but various groups have tested for cytotoxicity during their investigations. MTT (methyl thiazolyl tetrazolium) assays have been used to study cell toxicity by measuring the conversion of MTT to a different species. This occurs in the presence of functioning mitochondria. The conversion turns yellow MTT to dark blue. Absorbance measurements in the 500-600 nm range show an inverse relationship between toxicity and absorbance. In the previously mentioned Au-LA NCs, concentrations up to 150 μg/mL were found to not be toxic to HeLa cells over a span of 24 hours.[35] Glutathione stabilized Au NCs were shown to not exhibit toxicity effects at concentrations up to 400 μg/mL for human neuroblastoma (cancer) cells SH-SY5Y.[36] Human aortic endothelial cells (HAEC) did not show toxicity effects at up to 500 nM.[37] In addition to the MTT assay results, cell morphology was not noted to differ from healthy, untreated cells.

Nanocluster size is one factor that plays a role in whether or not the body is able to efficiently excrete the NCs after a period of time, a requirement by the FDA for any potential drug. Larger NPs, about 5.5 nm core diameter, have been shown to have good retention that would aid in the delivery of a treatment agent. Ligand structure affects the nonspecific accumulation of Au NCs with glutathione having been shown to minimize nonspecific binding for smaller Au NCs. Research into the ability to combine sufficient retention time for efficacy with nonspecific binding for renal-clearable Au NPs was performed using 2.5 nm Au-glutathione NPs. In that study, the Au NCs were found to have low uptake by healthy tissue while maintaining high concentrations in tumor prior to renal clearance.[1]

1.3 Objectives

The catalog of absorbance and emission properties of Au NCs of varying sizes continues to grow, but the jump from characterization to potential application in the fields of cellular imaging and drug delivery includes many questions that have not yet been answered. The role of nanocluster charge, size, ligand, and concentration are all known to play a factor in how or even if they make it into a cell. The following will describe research focused on enhancement of the quantum efficiency of near IR luminescent Au NCs and their potential application in cell imaging.

2 QUANTUM EFFICIENCY ENHANCEMENT OF MONOTHIOLATE Au NCs

2.1 Synthesis and thermo treatment

Separately, two monothiolate-stabilized gold nanoclusters (Au NCs) were synthesized by a modified Brust-Schiffrin method. Mercaptosuccinic acid (MSA) and tiopronin (Tio) were the water soluble monothiols used in the synthesis. Following synthesis and purification, the Au NCs

were heated in water with excess ligand thiol for one day. This thermo treatment was used to enhance the near IR luminescence of the synthesized Au NCs. The Au NCs were characterized by UV-visible absorbance and fluorescence spectroscopy. Purity of the Au NCs was qualitatively assessed by ^{1}H NMR. Enhancement of Au NCs quantum efficiency (QE) was also monitored by UV-visible absorbance and fluorescence spectroscopy. Au NCs composition was studied by both electrospray ionization (ESI) and matrix assisted laser desorption ionization (MALDI) mass spectrometry. Coupling of methoxypolyethylene glycol amine (PEG) to Au NCs was monitored by UV-visible absorbance and fluorescence spectroscopy followed by quantitative analysis with ^{1}H NMR.[38]

2.1.1 Monitoring changes in UV-visible absorbance and fluorescence

Figure 2 shows representative spectra after synthesis, but before thermo treatment, and after thermo treatment with excess free thiol. The absorbance curves were normalized at 300 nm, showing a decrease in absorbance. The fluorescence intensity increased with the thermo treatment as shown by the fluorescence spectra normalized at the excitation wavelength of 400 nm. Breaks in the wavelength axis represent emission intensity data gathered from two different detectors. Emission peak location at approximately 830 nm (Au-MSA) and 800 nm (Au-Tio) with a small shoulder at 900 nm for both did not shift during the heating procedure.

The synthetic and heating conditions were varied, as shown in Table 2. The synthesized Au-MSA and Au-Tio nanoclusters displayed relatively featureless absorbance spectra. Heating the NCs in the presence of excess ligand thiol resulted in a sizable increase in emission intensity without a shift in emission wavelength. Normalization of the absorbance spectra at 300 nm made noticeable a decrease in absorbance resulting from the heating treatment. From the normalized emission intensity spectra, it is clear the quantum efficiency increased significantly. As shown in

Table 2, the average enhancement factor of five was observed with a range of two to nine times the original quantum efficiency. Earlier it was discussed the onset of specific peaks in the absorbance spectrum corresponded with particular sizes of Au NCs when specific ligands, e.g. glutathione, were used during the synthesis. The continued relative featureless absorbance spectrum suggested the synthesized Au NCs were not a monodisperse solution. The focus on a general procedure for synthesizing Au NCs for later modification of the ligands led to the conclusion monodisperse products would not be necessary.

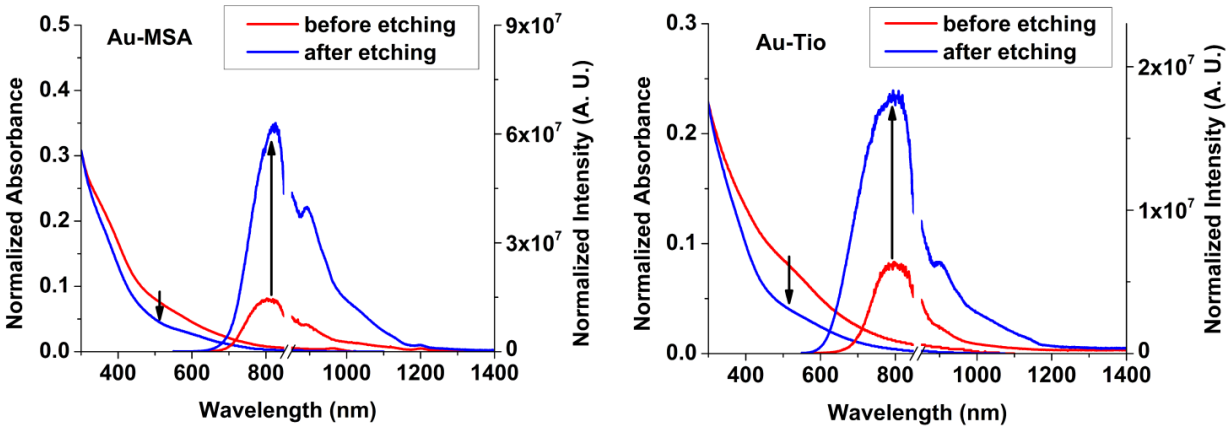

Figure 2. Normalized absorbance and normalized emission spectra before and after etching for Au-MSA nanocluster (left) and Au-tiopronin (right). The Au-MSA NCs (15X) and Au-Tio NCs were heated at 50 °C over 24 hours in the presence of 10X excess thiols respectively [reference 38– Reproduced by permission from The Royal Society of Chemistry].

Table 2. Summary of QE enhancement for varied parameters in synthesis and heating of Au NCs [reference 38– Reproduced by permission from The Royal Society of Chemistry].

Ligand	Ligand:Au synthesis ratio	Excess ligand added for etching	QE before etching (%)	QE after multi-step etching (%)	Enhancement factor after multi-step etching	Temperature & Duration
The impacts of different temperatures, three-day duration						
MSA	10	10x	0.7	2.8, 3.2, 2.7	4.0, 4.6, 3.9	**50 °C** for 2 days, **60 °C** for 3rd day
MSA	10	10x	0.8	2.2	2.8	**Room temperature** 3 days
The impacts of different thiol:nanocluster ratio, two-day duration						
MSA	3	**5x**	0.6	3.8, 4.1	6.3, 6.8	50 °C 24hrs, 48 hrs
MSA	3	**10x**	0.6	4.1, 5.1	6.8, 8.5	50 °C 24hrs, 48 hrs
MSA	3	**50x**	0.6	3.6, 3.4	6.0, 5.7	50 °C 24hrs, 48 hrs

Ligand	Ligand:Au synthesis ratio	Excess ligand added for etching	QE before etching (%)	QE after etching (%)	Enhancement factor	Temperature & Duration
Different Au nanoclusters from different thiol:Au synthetic ratio						
MSA	**3**	10x	0.3	1.6	5.3	50 °C 24 hours
MSA	**10**	10x	0.3	1.5	5.0	50 °C 24 hours
MSA	**15**	10x	0.4	3.3	8.2	50 °C 24 hours
Reproducibility from different batches						
MSA	15	10x	**0.8**	4.5	5.6	50 °C 24 hours
MSA	15	10x	**0.6**	4.0	6.7	50 °C 24 hours
MSA	15	10x	**1.7**	7.8	4.6	50 °C 24 hours
Different ligand						
Tiopronin	3	10x	**1.8**	6.6	3.7	50 °C 24 hours
Tiopronin	3	10x	**0.7**	4.1	5.9	50 °C 24 hours
Tiopronin	3	10x	**3.2**	5.4	1.7	50 °C 24 hours
Tiopronin	3.4	10x	**4.6**	9.8	2.1	50 °C 24 hours
Average enhancement factor					**4.9**	

The kinetics of QE enhancement due to heating was observed to level off after a span of one day, as shown in Figure 3. An increase in QE was also observed when excess ligand thiol was added and left to stir at room temperature, but the rate of increase was significantly slower. In the interest of expediency, the application of heat sped up the process. Representative excitation spectra before and after the heating procedure are shown in Figure 4. Varying the ratio of excess ligand thiol, as shown in Figure 5, showed a modest effect with 10X performing slightly better than 5X and 50X. Higher temperature (60 °C) or extended duration heating (2-3 days) did not significantly improve the QE, as shown in Figure 10 to be discussed shortly. Given the previous discussion on higher ratios of excess thiol and higher temperatures leading to etching of the core versus more mild conditions leading to annealing, it was decided to standardize the procedure at using 10X excess thiol ligand heated to 50 °C for 24 hours.

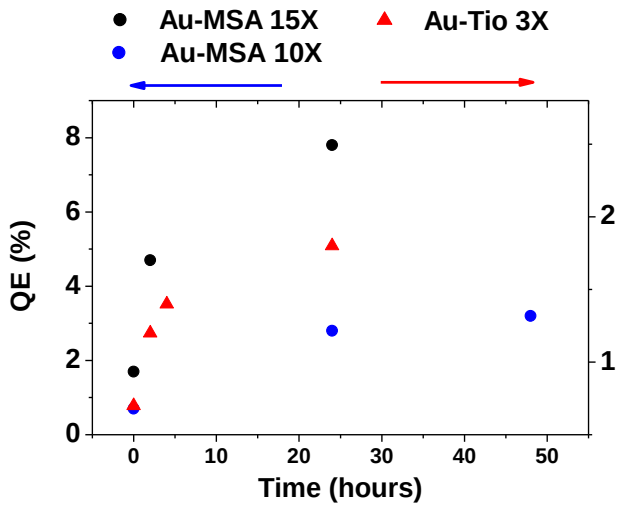

Figure 3. Kinetics of QE changes upon heating at 50 °C in the presence of additional free thiols (10X). Each measurement was taken once with explanation in body of text. [reference 38– Reproduced by permission from The Royal Society of Chemistry].

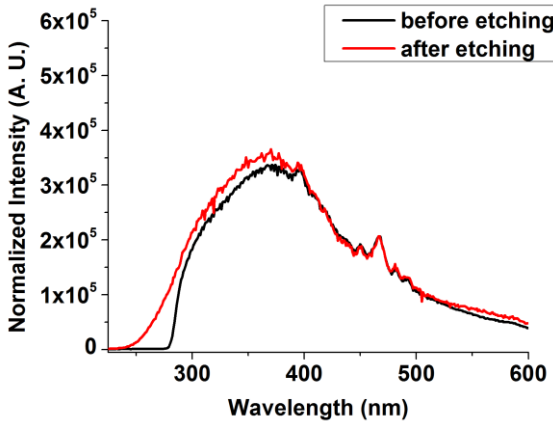

Figure 4. Excitation spectra of Au-Tio NCs before and after heating treatment with excess thiol ligand. Spectra normalized at 467 nm to illustrate similarity [reference 38– Reproduced by permission from The Royal Society of Chemistry].

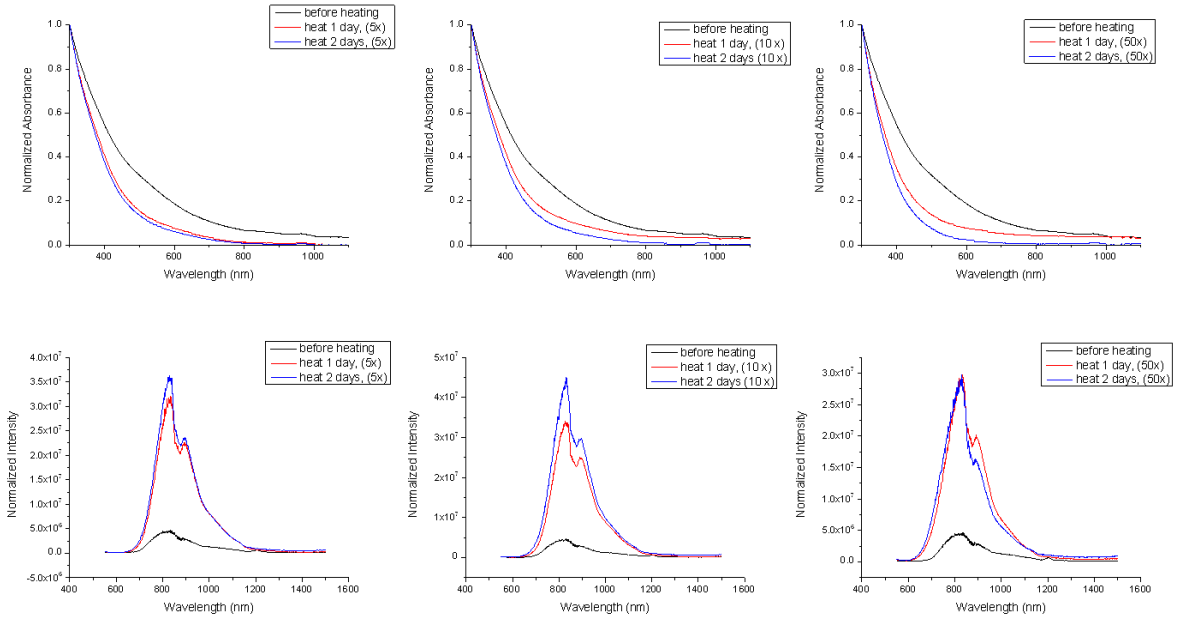

Figure 5. Normalized absorbance (top) and normalized emission (bottom) spectra of Au-MSA NCs before, during, and after heating treatment with varied ratios of excess ligand thiols [reference 38– Reproduced by permission from The Royal Society of Chemistry].

It is worth noting the variability noticed in QE values in Table 2. Variability can partly be attributed to synthesis of various batches having been performed by multiple individuals, but generally it was the same individual for examining a specific variable, e.g. thiol ratio during synthesis. This variability also prevented the aggregation of before, during, and after treatment data for the inclusion of error bars in Figure 3. Despite the variability, the heating procedure on aver-

age enhanced the QE by a factor of about five. The density of states (DOS), looking at the degree of absorbance curvature decay, was examined for the various batches by looking at the absorbance at 400 nm after normalization at 300 nm. Figure 6 shows a plot of this DOS versus QE for individual measurements before and after treatment, thus the dashed lines to clarify the connection between pairs of data points rather than solid lines that would imply the possible interpolation between the points. It was curious to note the before and after heating treatment lines from one batch to another, despite differences in before and after QE, were nearly parallel. Cross-over and convergence of the lines would be expected if the gold core was being etched to a smaller size. Also, the lack of appearance in discrete absorbance peaks suggested the samples were not becoming more monodisperse. It was thus assumed the provided ratio of thiols and accompanying energy were insufficient to modify the less stable species and leave behind a lower variety of different, more thermally stable NCs. Thus it was proposed the enhancement in QE was primarily due to the heating procedure optimizing the ligand arrangement around the Au core.

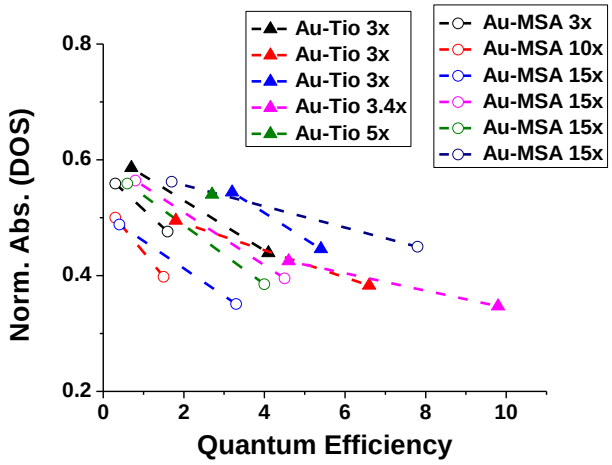

Figure 6. The changes in absorption curvature and QE upon heating for individual batches of Au NCs. The absorbance value at 400 nm was used as Norm. Abs. to reflect the curvature, or DOS, by normalizing the absorbance at 300 nm to 1 in each corresponding spectrum. No error bars shown for reasons discussed in section 2.1.1 [reference 38– Reproduced by permission from The Royal Society of Chemistry].

The previously mentioned observations of varied ligand thiol ratios, extended heating durations, and letting solution stir at room temperature can been seen in Figure 7. Heating the solution for three days or using a significant excess of free ligand thiol, i.e. 50X, both led to a sudden change in direction due to a decrease in QE after the first day. It is possible core etching of at least some of the core sizes was the cause. Also of note, the room temperature treated sample was slowly undergoing a similar process to those heated to 50 °C, but the tradeoff in allotted time for an optimally enhanced sample made heating favorable.

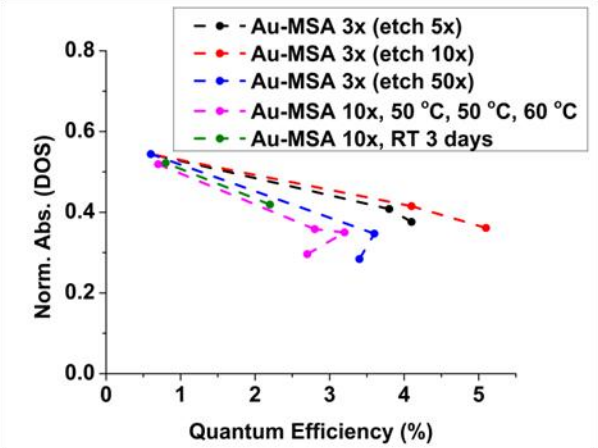

Figure 7. The changes in absorption curvature and QE upon heating at higher ratios free ligand thiol, for longer duration, or at room temperature for individual batches of Au NCs. No error bars shown for reasons discussed in section 2.1.1[reference 38– Reproduced by permission from The Royal Society of Chemistry].

2.1.2 Lack of change in ^{1}H NMR

This argument of ligand optimization, rather than core etching, is further supported by the modest changes in the NMR spectra shown in Figure 8. The previously mentioned line broadening effect is evident. The similarity between the before and after heating procedure samples, e.g. peak locations and full width at half maximum, are readily apparent. If the core was etched to a smaller size, the change in local environment should have been visible by a change in the line broadening effect. The same similarity between before and after ^{1}H NMR spectra were also observed for Au-MSA NCs. One small difference, the splitting of the methyl peak for Au-Tio NCs,

was previously reported. The splitting was attributed to two slightly different environments the ligands occupied on the Au core surface.[39]

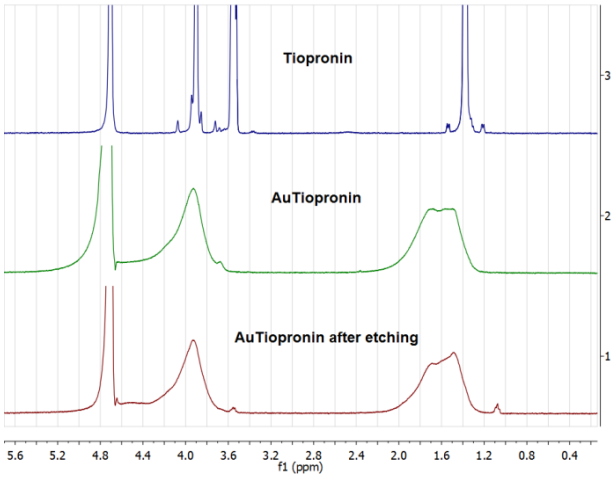

Figure 8. ^{1}H NMR spectra of tiopronin protected gold nanoclusters before (green) and after (red) etching with excess tiopronin (blue, free tiopronin molecules) at 50 °C for 24 hours [reference 38– Reproduced by permission from The Royal Society of Chemistry].

2.1.3 Mass spectrometry

Elucidation of particle composition was attempted by mass spectrometry, but conclusive results have thus far not been obtained. Electrospray ionization (ESI) was attempted given the possibility for multiple charges to be easily established with so many carboxylic acids present on the NCs. The major peak at 1383 m/z corresponded to a Au_4MSA_4 fragment, as shown in Figure 9, with Na^+ adducts observed at whole number multiples of +22 m/z. Significant fragmentation was observed using matrix-assisted laser-desorption-ionization (MALDI). The appearance of a Au_xS_y species with the thiol-carbon bonds broken, as has been observed by other groups using MALDI, was not detected. What was observed was a spacing of approximately 149 m/z over the range 2000-4000 as shown in Figure 10. This suggested either MSA was being lost, by breaking of the Au-S bond, or a rather polydisperse sample of Au-MSA NCs. In either case the results were inconclusive.

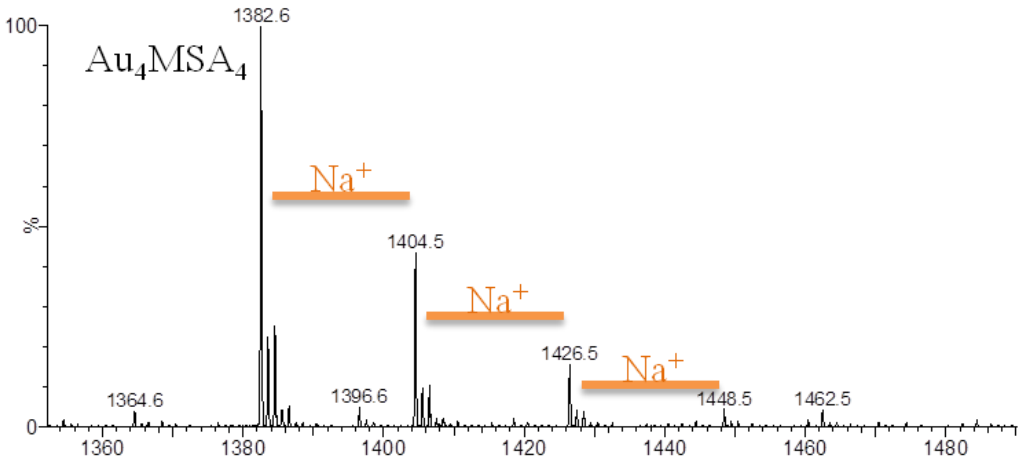

Figure 9. ESI-Q-TOF mass spectrum of Au-MSA nanoclusters under negative mode. Peak at 1383 m/z corresponds to Au_4MSA_4 fragment with visible H^+-Na^+ ion exchange patterns (+/- 22 m/z) [reference 38– Reproduced by permission from The Royal Society of Chemistry].

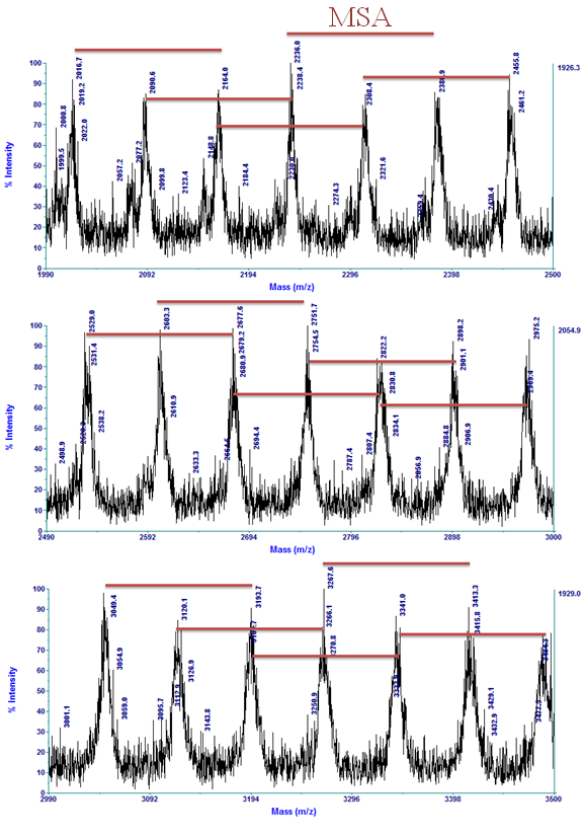

Figure 10. MALDI mass spectra of Au-MSA NCs. Note the red bars illustrate uniform spacing at ca. 149 m/z between peaks that corresponds to a difference of the MSA ligand. Data collected under linear negative mode using CHCA as matrix [reference 38– Reproduced by permission from The Royal Society of Chemistry].

2.1.4 pH/buffer effect on quantum efficiency

The application of gold nanoclusters to cell studies necessitates understanding how fluctuations in pH and ionic strength from one microenvironment to another affect the luminescent properties of the NCs. The quantum efficiency of Au-MSA NCs was observed to be relatively consistent, over a range of pH 5-9 as shown in Figure 11, when HCl or NaOH were used to adjust the pH of unbuffered nanopure water. A slight increase in QE was observed at higher pH as the polarity of the ligand monolayer was increased with the deprotonation of the carboxylic acids at higher pH, but that level of resolution was not studied in detail. The single significant figure QE values led to a consideration of two points within one percentage point being close to the same.

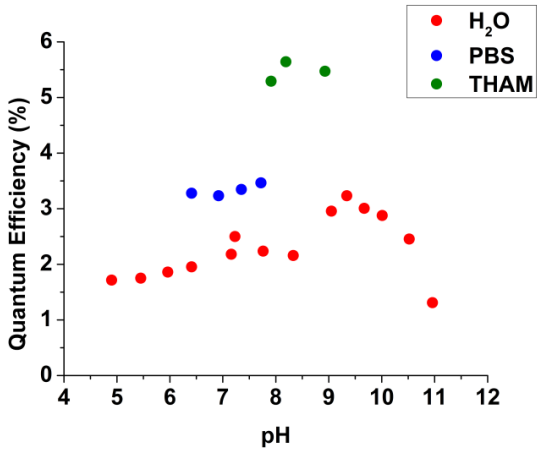

Figure 11. The dependence of QE on solution pH and buffer. The Au-MSA NCs (15X) was heated at 50 °C for 24 hours in the presence of excess MSA thiol (10X) and purified prior optical measurements. Each measurement was taken once with explanation in body of text [reference 38– Reproduced by permission from The Royal Society of Chemistry].

Buffer systems are used in animals to maintain the necessary pH range for proper function, and cell studies employ buffer systems for the same purpose. Au-MSA NCs in 0.1 M buffer systems of phosphate buffered solution (PBS) and tris(hydroxymethyl)aminomethane (THAM) had a higher QE than in nanopure water. It was proposed at higher ionic strength the buffers were increasing the deprotonation of the carboxylic acids. A higher QE with THAM versus PBS

or nanopure water was attributed to a better screening of the monolayer to ion intrusion. A proof of concept experiment, as shown in Figure 12, by titrating PBS and THAM into a solution of Au-MSA NCs and comparing the QE relative nanopure water. The resultant 1.2 and 1.8 QE factors for PBS and THAM, respectively, relative to nanopure water were observed and found to quickly plateau at low milli-molar concentrations. These two results were consistent with the observations in prototype PBS and THAM buffers. The difference in magnitude of change was likely due to variation between batches of Au-MSA NCs.

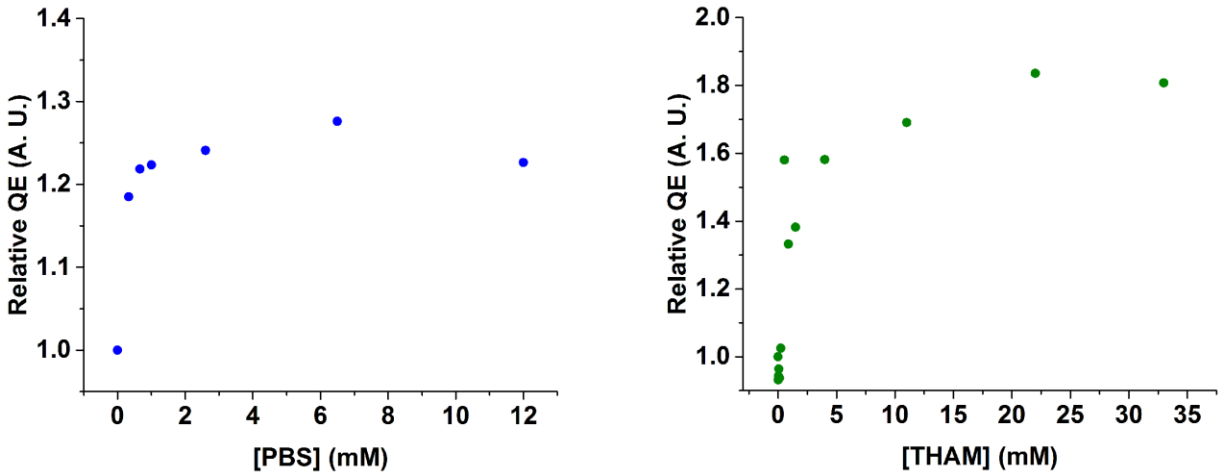

Figure 12. Relative QE of Au-MSA nanoclusters dissolved in water and titrated with PBS or THAM. Proof of concept titrations with one measurement each [reference 38– Reproduced by permission from The Royal Society of Chemistry].

2.1.5 Titration with Ca^{2+} and Mg^{2+}

Titration of Au-MSA NCs with Ca^{2+}, as shown in Figure 13, led to a minor upward shift in absorbance, suggesting a small amount of suspended material as more Ca^{2+} was titrated into solution. It was also observed by a small increase in the emission baseline at shorter wavelength. At the same time, emission intensity of Au-MSA NCs decreased as more Ca^{2+} was titrated into solution along with an increase in baseline intensity. Titration of Au-MSA NCs with Mg^{2+}, as shown in Figure 14, had a more pronounced downward effect on emission intensity and increase in baseline emission. A minor upward shift in absorbance was also observed. These observations

differ from what was reported for glutathione stabilized gold nanoclusters. In that report, nanoclusters emission intensity was not affected by either Ca^{2+} or Mg^{2+}. Several other divalent cations were tested, but only Cu^{2+} showed a marked decrease in emission intensity.[32]

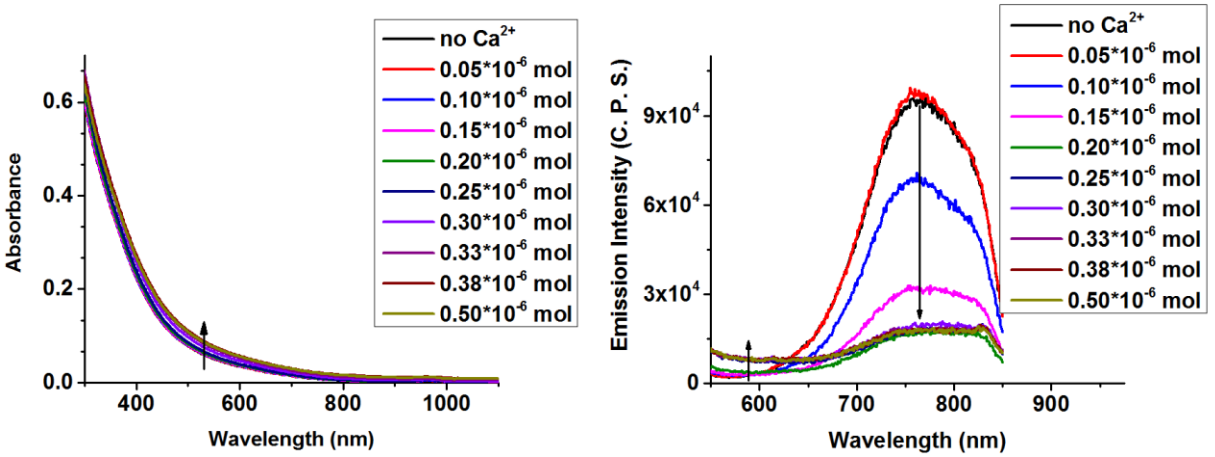

Figure 13. Absorbance (left) and luminescence (right) spectra of Au-MSA NCs during titration with $CaSO_4$.

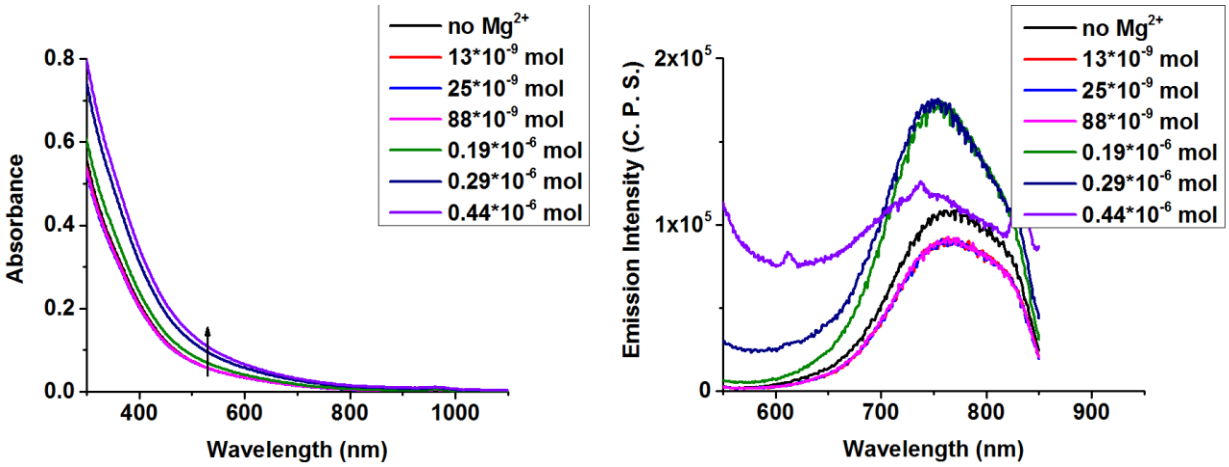

Figure 14. Absorbance (left) and luminescence (right) spectra of Au-MSA NCs during titration with $MgSO_4$.

2.2 Coupling reaction with methoxypolyethyleneglycol amine

As previously discussed, Au NCs with charged ligand functional groups interact with the components of cell growth media to form a protein corona surrounding the Au NCs. Coupling of compounds to inhibit nonspecific binding have been shown effective to minimize these non-

covalent interactions. In the case of Au-MSA and Au-Tio NCs, the coupling agent of choice was methoxypolyethyleneglycol amine (PEG) with a molecular weight of 750 g/mol.

2.2.1 Coupling reaction

Though discussed in more detail in the appendix, the primary amine of PEG was coupled to the carboxylate of the ligand using an excess of the coupling agent N-(3-dimethylaminopropyl)-*N'*-ethylcarbodiimide hydrochloride (EDC) in slightly basic nanopure water, as shown in Figure 15. The relative coverage of ligands with PEG was monitored by luminescence intensity as discussed in the next section.

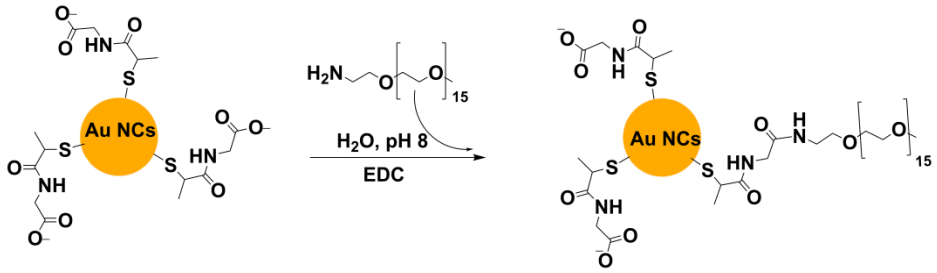

Figure 15. Cartoon of coupling reaction to attach PEG to tiopronin carboxylate of Au-Tio NCs.

2.2.2 Decrease in quantum efficiency

As shown in Figure 16, coupling PEG to Au-MSA NCs had no discernible effect on the absorbance spectra and the same was observed for Au-Tio NCs as shown in Figure 16. The emission wavelength also did not change, but the intensity of the emission, or quantum efficiency, did decrease. The amount of coupling of the amine terminated PEG to the ligand carboxylates determined the reduction in QE of the Au NCs. This was analyzed by looking at the ^{1}H NMR, as shown in Figure 17, for the NCs and comparing the area of the MSA CH_2 around 3.1 ppm versus the repeating CH_2CH_2O of PEG at 3.6 ppm. As the ratio of PEG:MSA increased from 1:40 to ca 1:1 (full coverage of MSA with PEG), the QE decreased from the original value to negligible, as shown in Figure 18. Note a linear relationship is not claimed but merely a general trend. A more detailed study of this relationship was not a focus of this study due to the

readily apparent lack of later utility for higher ratios of coupling for the purpose of cell imaging. This reduction in QE with increased PEGlation meant it would be necessary to balance the tradeoff between nonspecific binding and a strong enough emission signal for confocal fluorescence imaging.

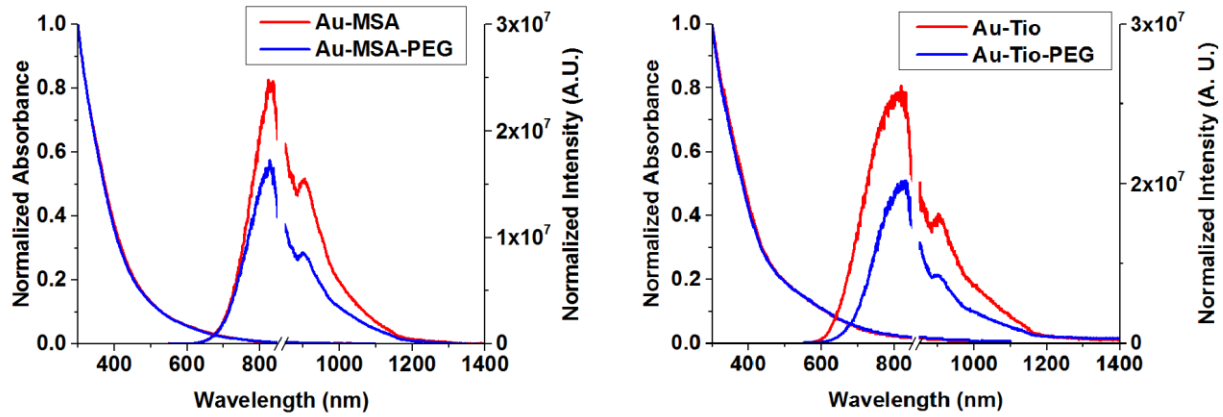

Figure 16. Normalized absorbance and normalized luminescence spectra of Au-MSA and Au-Tio NCs before and after coupling reaction with methoxypolyethylene glycol amine [reference 38– Reproduced by permission from The Royal Society of Chemistry].

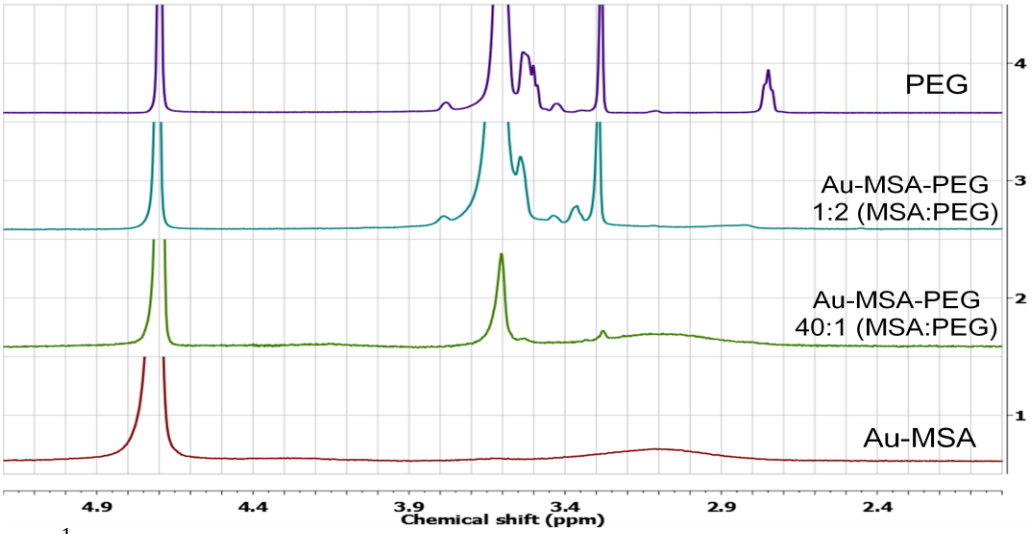

Figure 17. ^{1}H NMR spectra of Au-MSA nanoclusters before (red), after varied fractions of coverage with PEG (green, blue), and free PEG (purple) [reference 38– Reproduced by permission from The Royal Society of Chemistry].

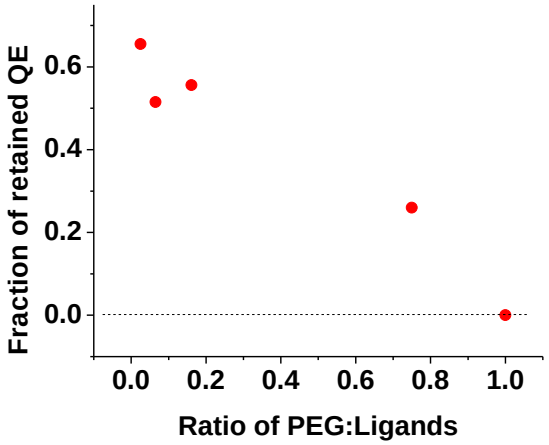

Figure 18. The dependence of QE on the fraction of PEGlation of ligands. Lack of error bars discussed in text [reference 38– Reproduced by permission from The Royal Society of Chemistry].

2.2.3 Quantum efficiency in cell growth media

Potential application of Au-MSA-PEG NCs in cellular imaging would require the NCs to remain sufficiently fluorescent while in a complex biochemical environment. Cell growth media, contents of which include Ca^{2+} and Mg^{2+}, thus merited investigation as to whether or not a similar response would occur as had for the divalent cation titrations.

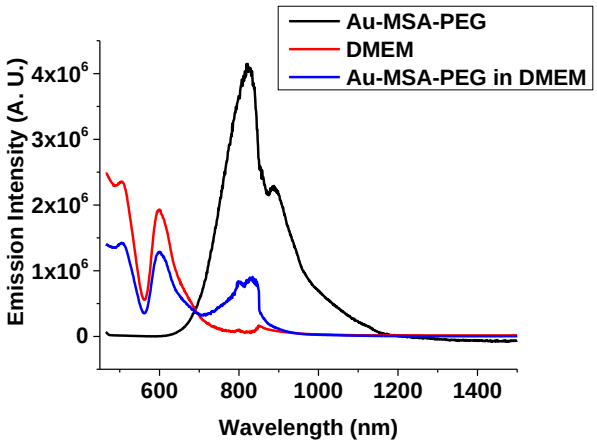

Figure 19. Emission spectra of Au-MSA-PEG NCs in water (black), cell growth media (red), and Au-MSA-PEG in cell growth media (blue).

A significant decrease in Au-MSA-PEG emission intensity was observed in cell growth media, as shown in Figure 19, when compared to when dissolved in water. While the NCs did

remain luminescent, the experiment indicated Au-MSA-PEG NCs detection would require consideration of NCs emission intensity. Sufficient PEGlation to limit the effect of protein corona formation versus sufficient emission intensity for detection by the confocal microscope detector meant a relatively low fraction of PEGlated ligands would be desirable for initial cell imaging studies.

3 FUNCTIONALIZATION OF DITHIOLATE STABILIZED Au NCs

3.1 Coupling reaction with polyethyleneglycol amine

Au-LA NCs were PEGlated much like how the previously discussed Au-MSA and Au-Tio NCs PEGlation occurred, as shown in Figure 20. Using Au-LA NCs recently discussed in the literature, coupling PEG to Au-LA NCs had the opposite effect as observed with Au-MSA and Au-Tio NCs, increasing rather than decreasing the QE.[40] This effect was relatively modest and not studied in greater detail. A similar trend will be shown in the next few sections.

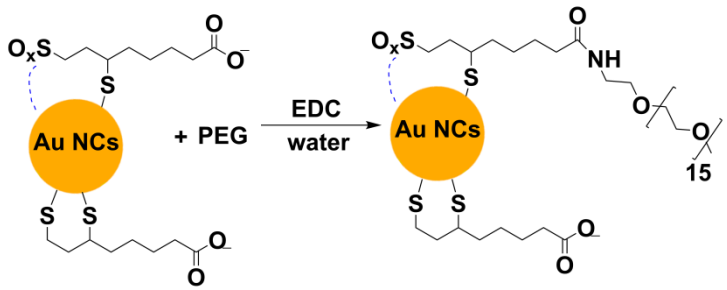

Figure 20. Cartoon of coupling reaction to attach PEG to lipoic acid carboxylate of Au-LA NCs.

3.2 Coupling reaction with monosaccharide rhamnose derivative

In collaboration with another group, a derivative of the carbohydrate rhamnose, with a primary amine at the end of a propyl spacer, was coupled to Au-LA NCs as shown in Figure 21.

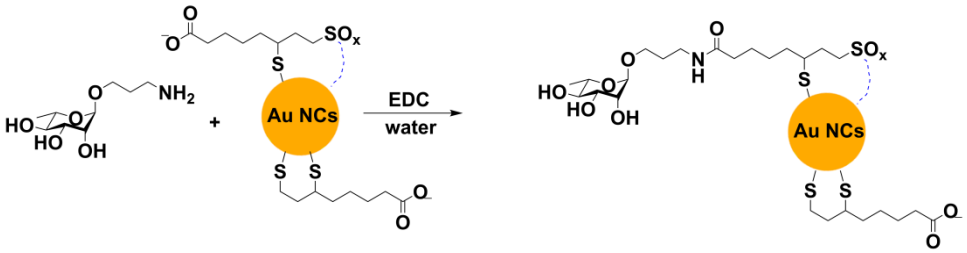

Figure 21. Cartoon of coupling reaction to attach rhamnose to lipoic acid carboxylate of Au-LA NCs.

As shown in Figure 22, absorbance did not change while a minor increase in emission intensity was observed. A separate coupling reaction of rhamnose to Au-LA NCs, at a higher ratio of rhamnose to NCs and shown in Figure 23, showed an emission increase that was more substantial. Why the lower ratio coupling reaction did not produce a comparable increase despite three times the duration was not investigated. It is possible the lower ratio resulted in lower coverage, but the amount of total material led to a poor ^{1}H NMR signal that was less than favorable for quantitative analysis.

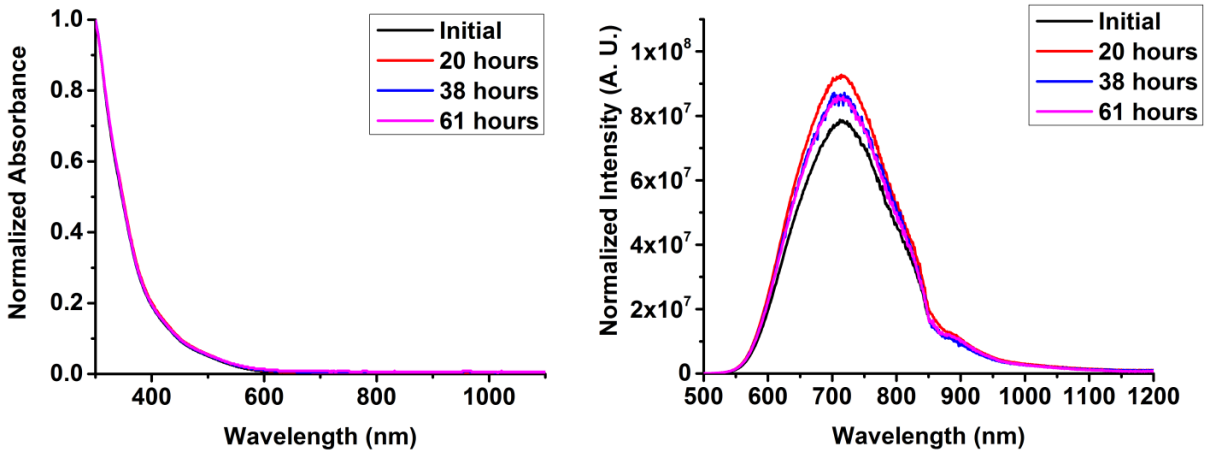

Figure 22. Normalized absorbance (left) and normalized luminescence (right) spectra of Au-LA NCs before and during coupling reaction with rhamnose.

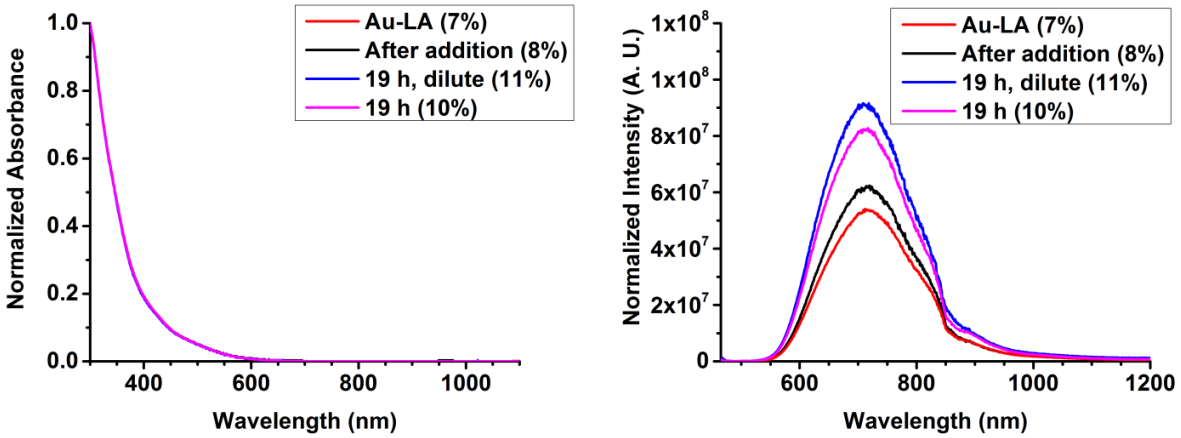

Figure 23. Normalized absorbance (left) and normalized luminescence (right) spectra of Au-LA NCs before and during coupling reaction with rhamnose.

3.3 Formation of Au-LA-zwitterion

Based on the previously discussed observations of amine coupling to Au-LA NCs at least slightly increasing emission intensity, a trend opposite to that observed with the monothiolate Au NCs, as the negatively charged carboxylate was replaced with a neutral amide. It was hypothesized that establishing a permanent positive charge on the ligand may increase the QE. To test the theory, a previously reported two-step coupling reaction was attempted.[41] As shown in Figure 24, the first step involved coupling N', N'-dimethylethane-1,2-diamine (diamine) to the lipoic acid carboxylate of Au-LA NCs to form the amide plus leave a tertiary amine further from the core. The second step, as will be discussed later, was not attempted.

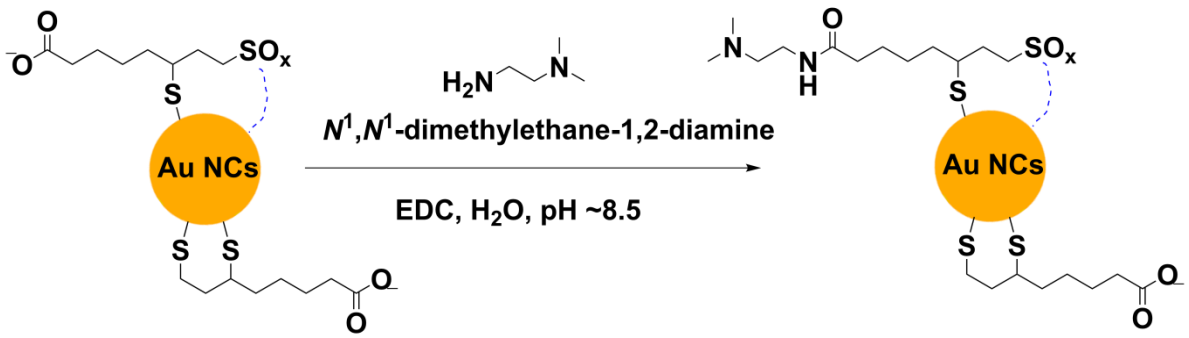

Figure 24. Cartoon of coupling reaction to couple 1,2-diamine to lipoic acid carboxylate of Au-LA NCs.

The absorbance spectra, as shown in Figure 25, shows that after three days solubility had started to be a problem. Emission intensity had increased a small amount, similar to the previous Au-LA NCs observations, with a decrease in emission after three days likely due to the solubility issue. Upon closer inspection, shown in Figure 26, the difference in QE between the product and the Au-LA NCs was negligible.

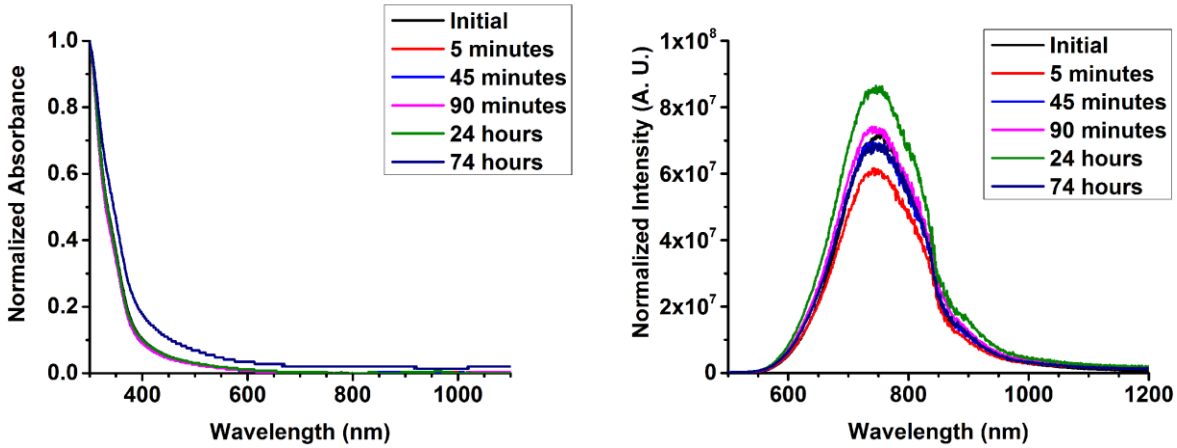

Figure 25. Normalized absorbance (left) and normalized luminescence (right) spectra of Au-LA NCs before and during coupling reaction with diamine.

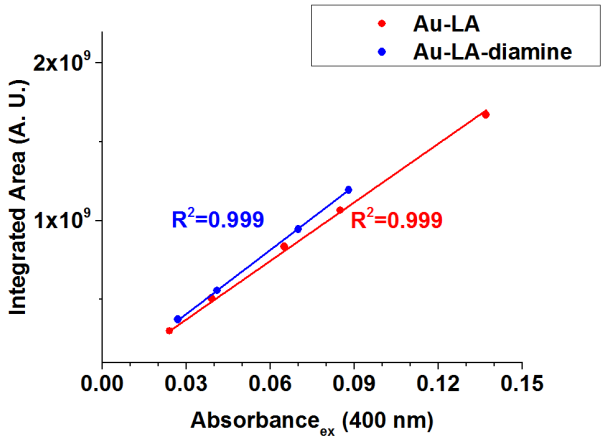

Figure 26. Integrated area vs. absorbance at excitation of Au-LA NCs and Au-LA-diamine NCs. A proof of concept experiment that was not studied in more detail for reasons discussed in section 3.3.

^{1}H NMR was used to determine whether or not the diamine had coupled onto Au-LA NCs. Most of the peaks in the 4.0-1.5 ppm region, shown in Figure 27, correspond to the lipoic acid ligand. The lipoic acid peaks in the 3.8-3.0 ppm region are typically small and difficult to

see due to their proximity to the gold core, but the observed peaks in this region appear to be from the diamine. Also, the peaks at approximately 2.8 and 1.1 ppm appear to be from the diamine. An additional attempt at purification should have been performed to see if the ^{1}H NMR spectra changed in order to verify purity. As such, no additional analysis of the Au-LA-diamine NCs NMR was performed.

Solubility issues of the Au-LA-diamine product became an issue when attempting the follow on reaction. Water as solvent worked for dissolving the NCs, but a previous attempt at this reaction suggested the coupling reaction did not succeed. Attempts to find a suitable nonaqueous solvent included the use of ethanol, methanol, acetone, and THF. Also attempted was a phase transfer from aqueous to more nonpolar solvents, e.g. dichloromethane, toluene, chloroform, without the aid of a phase transfer catalyst, but no NCs were transferred based on no difference in absorbance from baseline. The combination of no observed change in luminescence intensity, along with the poor solubility of the product, led to the decision to set the idea aside. Thus more extensive measurements were not attempted to clarify either the optical properties or fraction of coupled ligands.

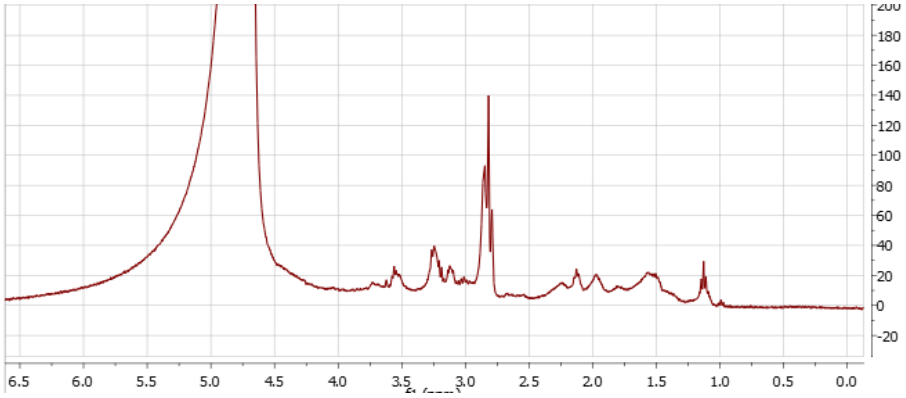

Figure 27. **^{1}H** NMR spectra of Au-LA-diamine NCs.

3.4 Coupling poly-l-lysine to Au-LA

Another possible route for establishing a permanent positive charge on the ligand was to couple poly-l-lysine in a similar manner to the PEGlation reactions. One concern was the presence of many primary amines on poly-l-lysine and the possibility for cross-coupling.

3.4.1 Titration of Au-LA NCs with poly-l-lysine

The first test was to see what would happen if poly-l-lysine was merely added to a solution of Au-LA NCs. As shown in Figure 28, Au-LA NCs were titrated with poly-l-lysine. No change in either absorbance or emission spectra was observed with up to 4.5 equivalents poly-l-lysine relative to NCs. A prior titration, spectra not shown, with higher ratios saw an immediate change to cloudy from clear upon the addition of ten equivalents poly-l-lysine. This observation demonstrated cross-linking could be an issue when trying to couple the two components.

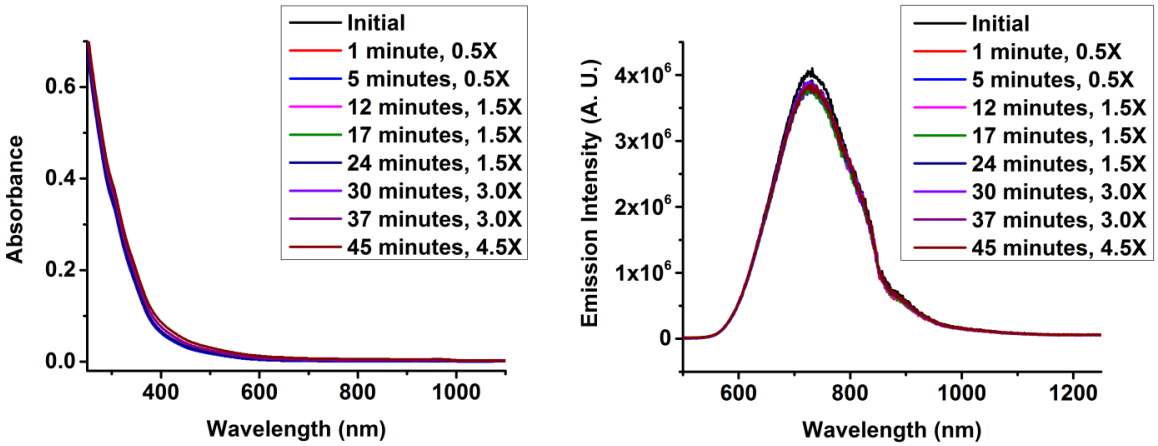

Figure 28. Absorbance (left) and luminescence (right) spectra of Au-LA NCs during titration with poly-l-lysine.

3.4.2 Coupling poly-l-lysine to Au-LA NCs

A small first attempt to couple poly-l-lysine to Au-LA NCs, using 5 equivalents per NCs, confirmed the prior observation. The reaction solution turned cloudy over time followed by loss of absorbance, emission, and solution color, spectra not shown. A second attempt, using a higher

ratio, 1.3 equivalents per ligand on Au-LA NCs, proceeded as shown in Figure 29. By 75 minutes the solution was cloudy and emission intensity had decreased. The absorbance spectrum had also significantly changed shape. After one day, emission intensity had further decreased, as had absorbance. The pH was adjusted with HCl and NaOH to determine whether it was a simple solubility issue. Though not shown in greater detail, the spectra were not that different for pH values 6.4 or lower. Lower absorbance and emission at pH 7.4 suggested solubility was one reason for the low signal intensity. The loss of emission intensity after three and a half days and a colorless solution indicated that pH only had a minor effect at earlier time points and was not the means by which to keep the resulting product from crashing out of solution. A much higher ratio of poly-l-lysine to NCs may limit the amount of cross linking, but it might be advisable to instead pursue a coupling reagent with not so many primary amines that complicate the reaction process.

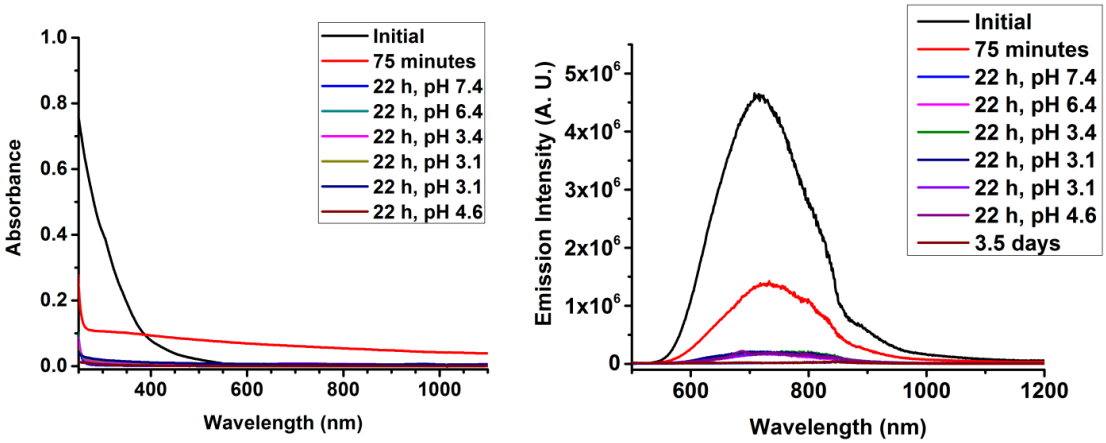

Figure 29. Absorbance (left) and luminescence (right) spectra of Au-LA NCs during coupling reaction with poly-l-lysine.

3.5 Monothiolate ligand addition/exchange with Au-LA NCs

The previously mentioned occurrence of ligand addition or exchange when gold nanoclusters are in solution with free thiols makes it worthwhile to see how resistant the Au NCs are to core-ligand changes. Biological systems have thiols, e.g. cysteine, that potentially may re-

act and change the function of the Au NCs. Au-LA NCs resistance to thiol addition/exchange were monitored by adding free thiol to a solution of Au-LA NCs and monitoring for changes in absorbance and luminescence.

3.5.1 Mercaptosuccinic acid

Fifteen equivalents of MSA, relative to NCs, was added to a solution and monitored. As shown in Figure 30, no change in absorbance was observed. The curvature remained the same, suggesting the particle was not being etched to a different size, and the absorbance at long wavelength remained consistent. The later indicates none of the particles transitioned from dissolved to suspended in the solution. Emission intensity remained relatively stable for up to 18 hours. Twenty five days later a decrease in emission intensity had been observed.

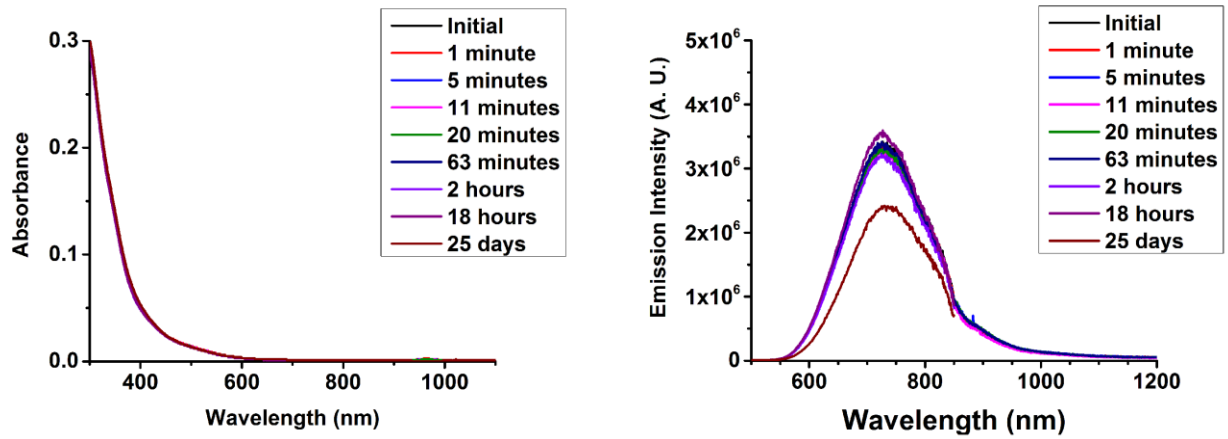

Figure 30. Absorbance (left) and luminescence (right) spectra of Au-LA NCs before and during exposure to fifteen equivalents of free mercaptosuccinic acid (MSA:Au-LA NCs).

That agrees with a separate experiment, not shown here, where at much higher concentrations MSA would start to alter Au-LA NCs over the span of a weekend. One of the observed changes was a reduction in luminescence QE. Another observation was NCs started to crash out of solution. Data is not presented here due to addition/exchange having occurred in an NMR tube over two weeks time frame.

3.5.2 Tiopronin

Similar to the previous addition/exchange experiment, fifteen equivalents of tiopronin, relative to the NCs, was added to a solution of Au-LA NCs and monitored with absorbance and fluorescence measurements. As shown in Figure 31, no change in absorbance was observed after twenty five days. No change in emission intensity was observed even after twenty-five days. It appeared that Au-LA NCs were more resistant to tiopronin addition or exchange than they were to MSA. A high concentration attempt, as performed with Au-LA NCs and MSA was not performed with tiopronin.

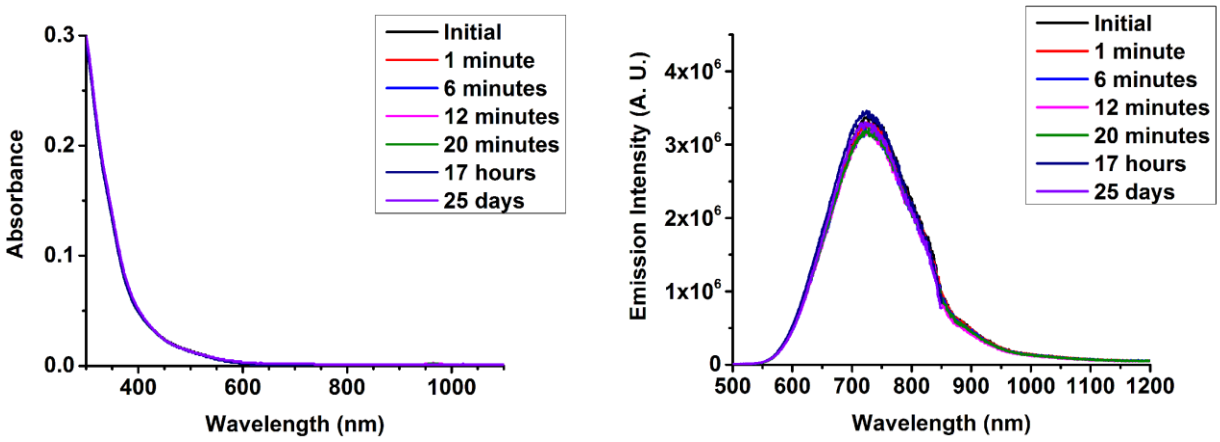

Figure 31. Absorbance (left) and luminescence (right) spectra of Au-LA NCs before and during exposure to fifteen equivalents of free tiopronin (tiopronin:Au-LA NCs).

3.5.3 Glutathione

Similar to MSA and tiopronin, glutathione was added to a solution of Au-LA NCs and monitored with absorbance and fluorescence measurements. In this case three equivalents of glutathione were added to a solution of Au-LA NCs. The absorbance spectra, as shown in Figure 32, with the exception of the three hour mark did not change after one day. The modest increase in absorbance for the three hour mark was noted for possible consideration later. The emission intensity remained stable for the first twenty minutes, with what appeared to be a slow decrease in intensity at the three and twenty eight hour marks.

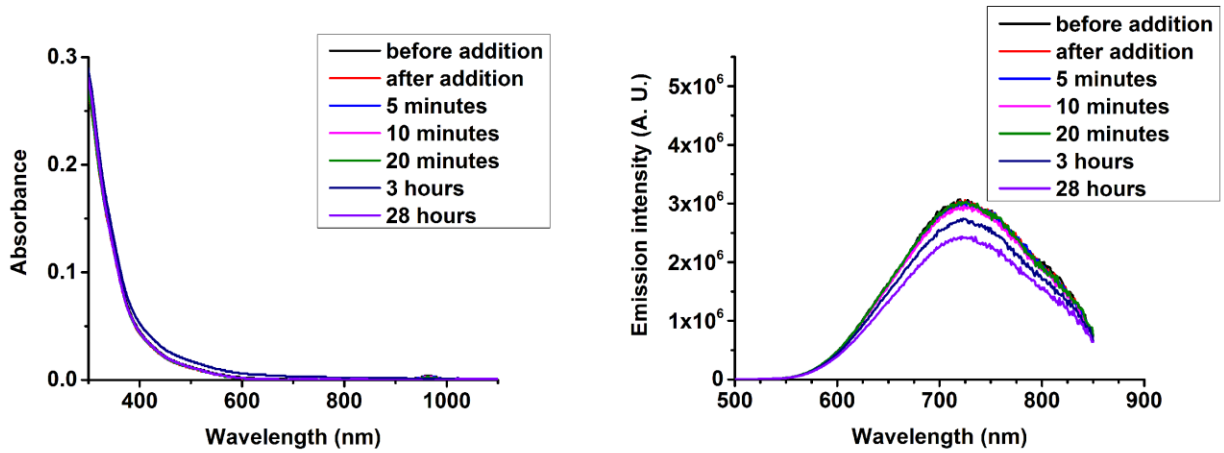

Figure 32. Absorbance (left) and luminescence (right) spectra of Au-LA NCs before and during exposure to three equivalents of free glutathione (glutathione:Au-LA NCs).

Based on the one time point change in absorbance and the slowly decreasing emission intensity, a second experiment with fifteen equivalents of glutathione were added to a solution of Au-LA NCs and monitored as previously mentioned. The higher ratio of glutathione, as shown in Figure 33, led to what appears to be a suspension in the solution, but no cloudiness was visually observed. Despite that, the emission intensity did not change within the first hour. Eighteen hours later a modest decrease in emission intensity was observed, but that was assumed related to the absorbance spectrum having decreased relative to the initial mark.

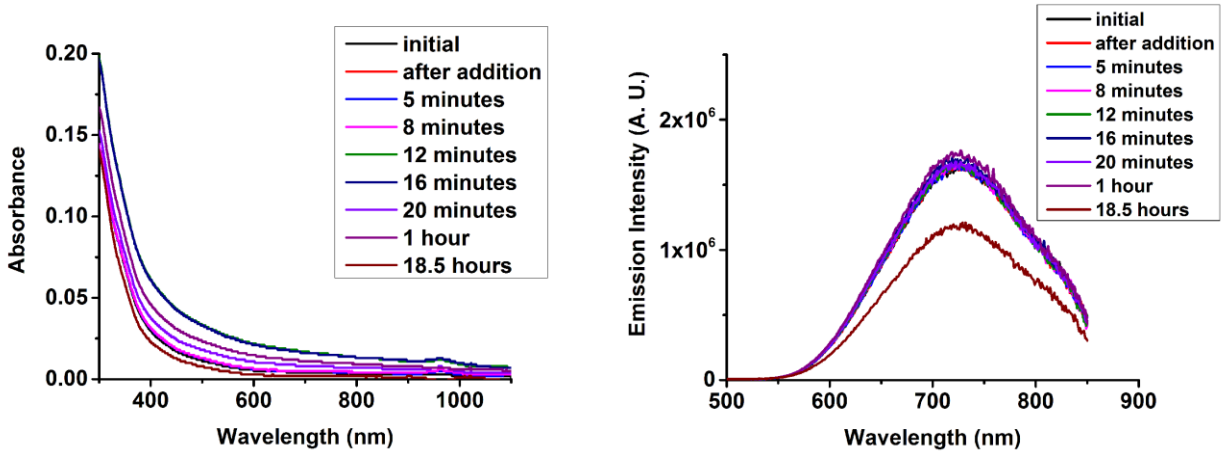

Figure 33. Absorbance (left) and luminescence (right) spectra of Au-LA NCs before and during exposure to fifteen equivalents of free glutathione (glutathione : Au-LA NCs).

The somewhat conflicting results between three and fifteen equivalents of glutathione suggest this thiol is reacting with the Au-LA NCs, but the result of that reaction is not clear. ^{1}H NMR measurements, which could elucidate what was occurring, were not taken due to the experiments involving too little material for a reasonable signal.

3.6 Titration with Ca^{2+} and Mg^{2+}

For the same reasons previously stated for Au-MSA and Au-Tio NCs, it was worth testing the effect of divalent cations on Au-LA NCs absorbance and emission. As shown in Figure 34, a titration of Ca^{2+} did not have the same effect on Au-LA NCs as observed for Au-MSA NCs. Absorbance and emission changed to a small extent, but not to the extent of becoming cloudy as previously discussed in an earlier section.

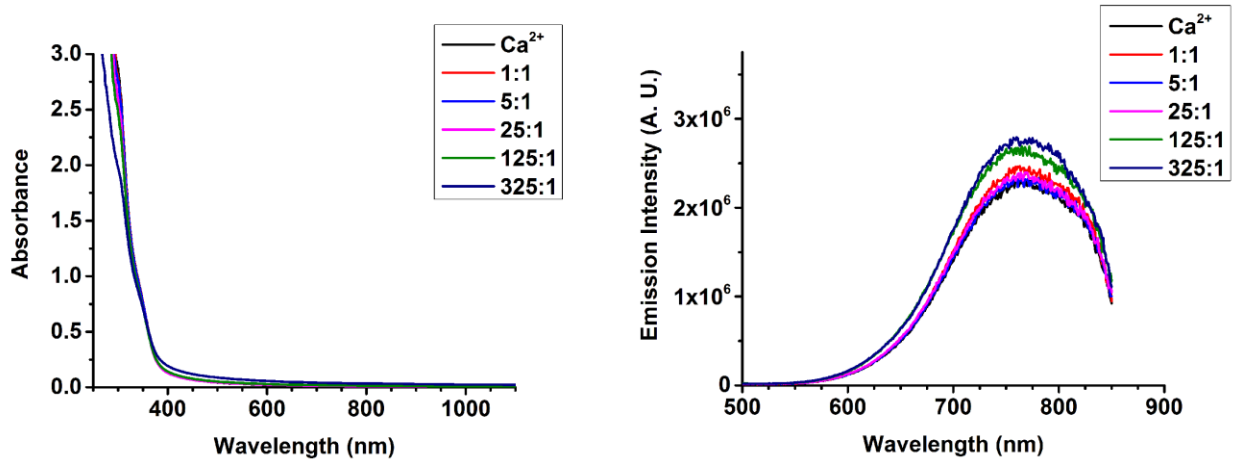

Figure 34. Absorbance (left) and luminescence (right) spectra of Au-LA NCs during titration with $CaSO_4$.

An even small effect was observed, as shown in Figure 35, when Mg^{2+} was titrated into a solution of Au-LA NCs. These two titrations suggested Au-LA NCs might be more suitable for cell imaging applications if one temporary does not consider localization inside the cell. The relative lack of change in emission intensity for Au-LA NCs better agreed with the report for Au-glutathione NCs.[32]

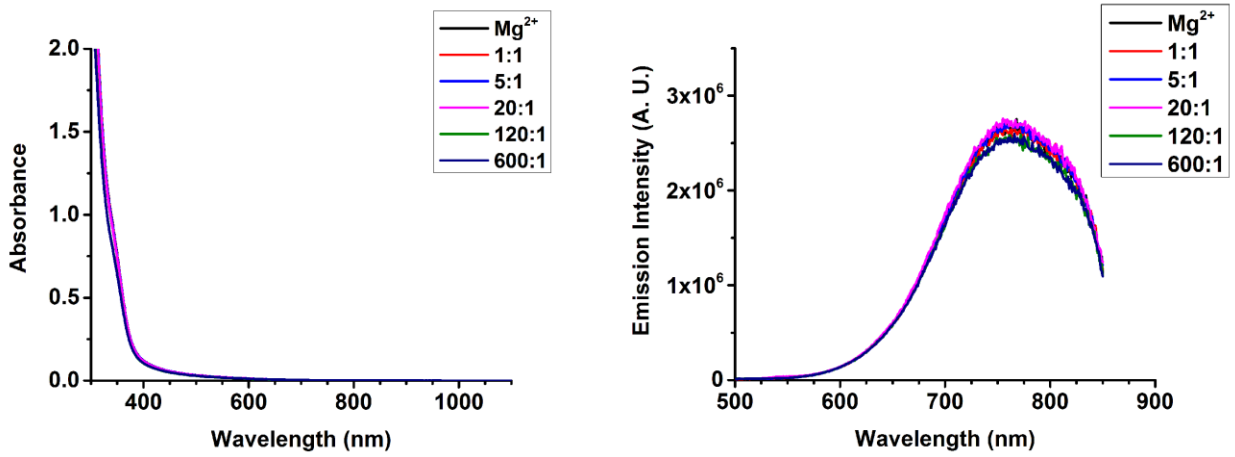

Figure 35. Absorbance (left) and luminescence (right) spectra of Au-LA NCs during titration with $MgSO_4$.

3.7 Quantum efficiency in cell growth media

The next step was to examine the effect of cell growth media. As shown in Figure 36, Au-LA NCs were first titrated into water with absorbance and emission measurements recorded. Next the same type of titration was performed, but the NCs were titrated into cell growth media. Cell growth media emission was subtracted from the titration data to obtain the emission due to the Au-LA NCs.

3.7.1 Au-LA NCs in cell growth media

The previously discussed Au-MSA-PEG NCs demonstrated a decrease in QE when dissolved in cell growth media versus nanopure water. A similar set of measurements were thus of interest for Au-LA NCs. Au-LA NCs were titrated into a solution of nanopure water, Figure 36, and separately similar concentrations of Au-LA NCs were titrated into cell growth media, Figure 37, with additional higher concentrations for the latter. A comparison of the two titrations, as shown in Figure 38, shows a possibly nonlinear increase in integrated intensity versus absorbance at the excitation wavelength when Au-LA NCs were dissolved in cell growth media. At the same time, however, their intensity in cell growth media was higher than when dissolved in

nanopure water. Additional titrations would be necessary to clarify the luminescence properties of Au-LA NCs in cell growth media versus water given the less than ideally linear results, but the titration was a proof of concept that showed dissolving Au-LA NCs in cell growth media did not significantly decrease their luminescence intensity the way it occurred when Au-MSA-PEG NCs were added to cell growth media. If future cell imaging studies progress past an initial investigative phase, then more detailed study of how these NCs respond to cell growth media will be beneficial.

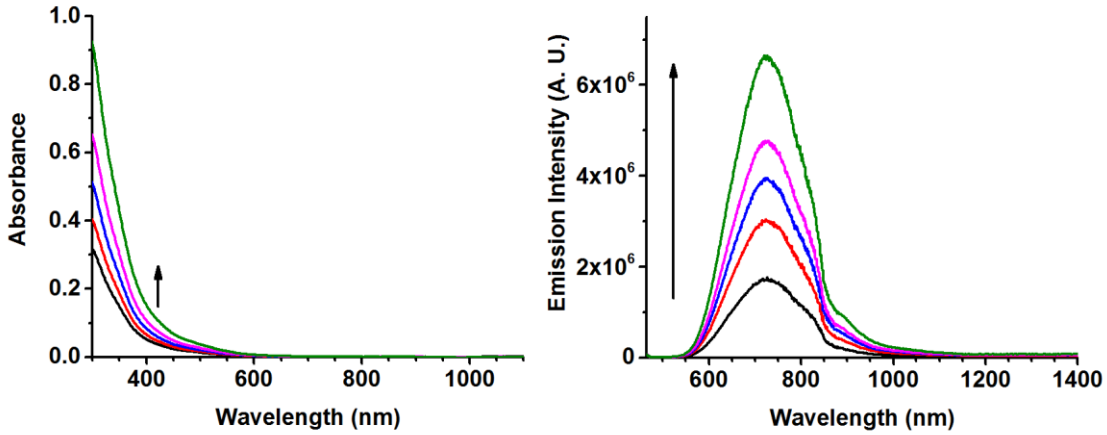

Figure 36. Absorbance (left) and luminescence (right) spectra as Au-LA NCs titrated into H_2O.

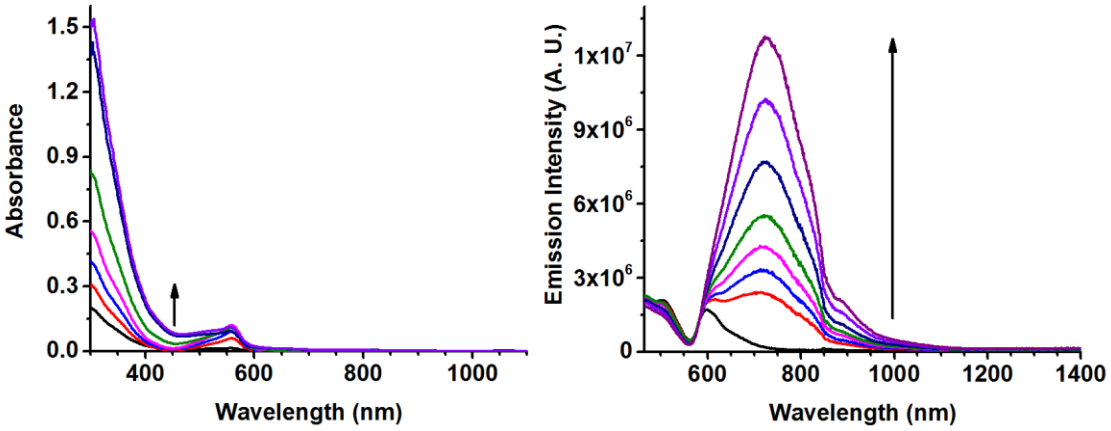

Figure 37. Absorbance (left) and luminescence (right) spectra as Au-LA NCs titrated into cell growth media.

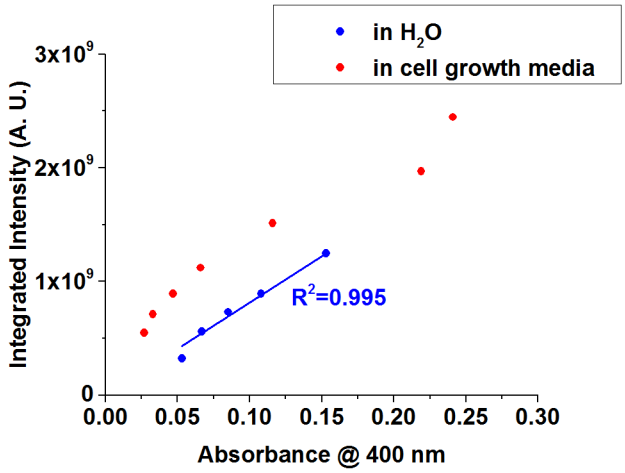

Figure 38. Integrated intensity versus absorbance at excitation of Au-LA NCs in nanopure water versus cell growth media in proof of concept titration. Data points were single measurements in a titration with a line of best fit added if a linear trend was observed. See section 3.7.1 for additional discussion.

3.7.2 Au-LA-PEG NCs in cell growth media

Comparing the water and cell growth media titrations, shown in Figure 39 and 40 respectively, Au-LA-PEG NCs initially had a slightly higher emission in cell growth media, but as NCs concentration increased the relative emission decreased relative to water. The linear response in water versus non-linear response in cell growth media, as shown in Figure 41, suggests Au-LA-PEG NCs are interacting with the media, but despite that the retained emission intensity is much higher than observed with Au-MSA NCs in cell growth media. The discussion in the previous section regarding the need for more detailed study of Au-LA NCs luminescence in cell growth media, should the initial investigative phase progress also applies to Au-LA-PEG NCs. Given the time involved to perform a dozen measurements of absorbance and fluorescence versus the time required for cell preparation, incubation, and fixation, the proof of concept titration demonstrated luminescence did not decrease to a point where cell imaging studies would not be worth pursuing. If this had not been the case, it would have been a small investment of time versus a more significant allotment of time.

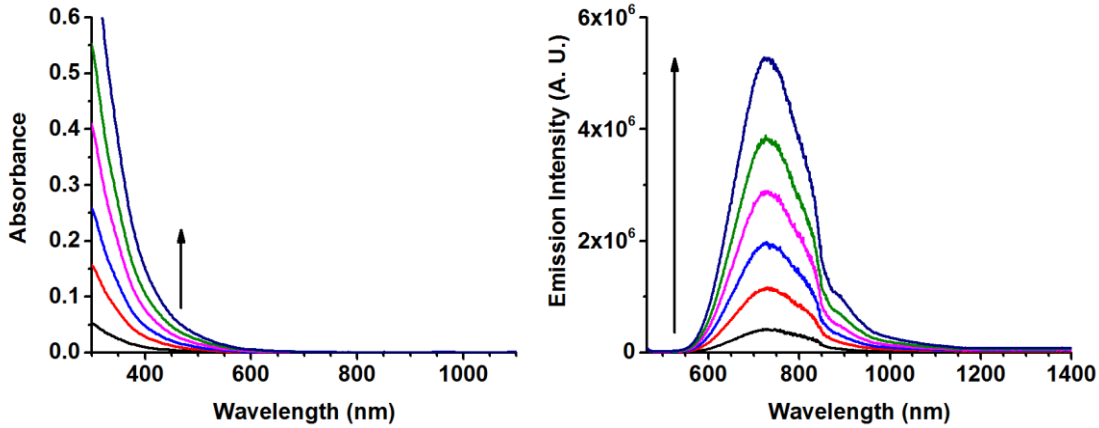

Figure 39. Absorbance (left) and luminescence (right) spectra as Au-LA-PEG NCs titrated into H_2O.

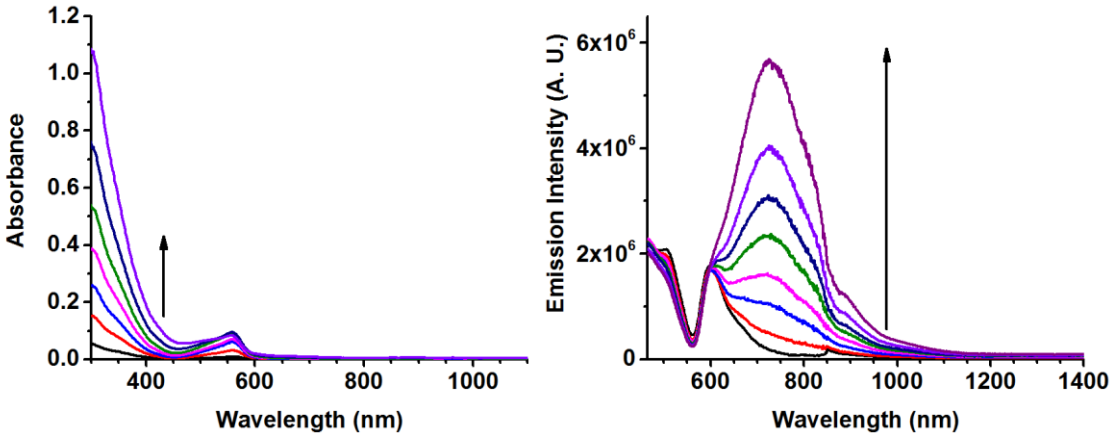

Figure 40. Absorbance (left) and luminescence (right) spectra as Au-LA-PEG NCs titrated into cell growth media.

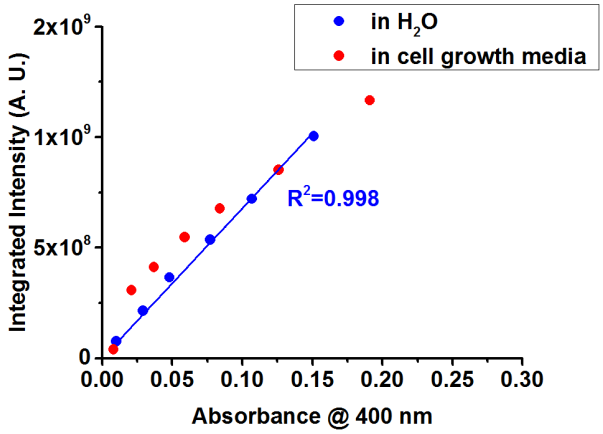

Figure 41. Integrated intensity versus absorbance at excitation of Au-LA-PEG NCs in nanopure water versus cell growth media in proof of concept titration. Data points were single measurements in a titration with a line of best fit added if a linear trend was observed. See sections 3.7.1 and 3.7.2 for additional discussion.

4 CONFOCAL IMAGING OF HELA AND HEK CELLS

Critical questions for potential applications of nanomaterials to biological uses are toxicity and long term retention. Previous reports of effective renal clearance of sub 5 nm Au NCs have been shown when the surface chemistry was properly designed.[1,42] The study of how luminescent Au NCs interact with human embryonic kidney cells (HEK) then becomes of interest for evaluating potential *in vivo* and *in-vitro* applications. Also of interest are potential differences in how Au NCs interact with healthy versus cancerous cells. This led to inclusion of HeLa (cervical cancer) cells for comparison to HEK cells.

4.1 Incubation method

HEK or HeLa cells were incubated at 37 °C with Au-MSA-PEG NCs in cell growth media for a set period of time. Following incubation, cells were washed in triplicate with PBS buffer and then fixation with 4% ice cold methanol at -20 °C for approximately five minutes. Next the cells were mounted on glass slides with Prolong Antifade reagent containing nuclear dye DAPI followed by another triplicate washing with PBS buffer.

4.2 Heterogeneous distribution in cytoplasm and nucleus

The Au-MSA-PEG NCs, with QE enhanced prior to PEGlation, were viable for direct imaging using a commercial confocal fluorescence microscope. As shown in Figure 42, Au-MSA-PEG NCs, shown in red, were heterogeneously distributed within individual HEK cells. The use of DAPI, a fluorescent dye used to stain DNA due to a high affinity to the A-T bases, allowed for colocalization of the two signals to show whether or not the NCs were making it into the nucleus. As shown in Figure 42, the two signals do overlap suggesting the NCs made it into the nucleus.

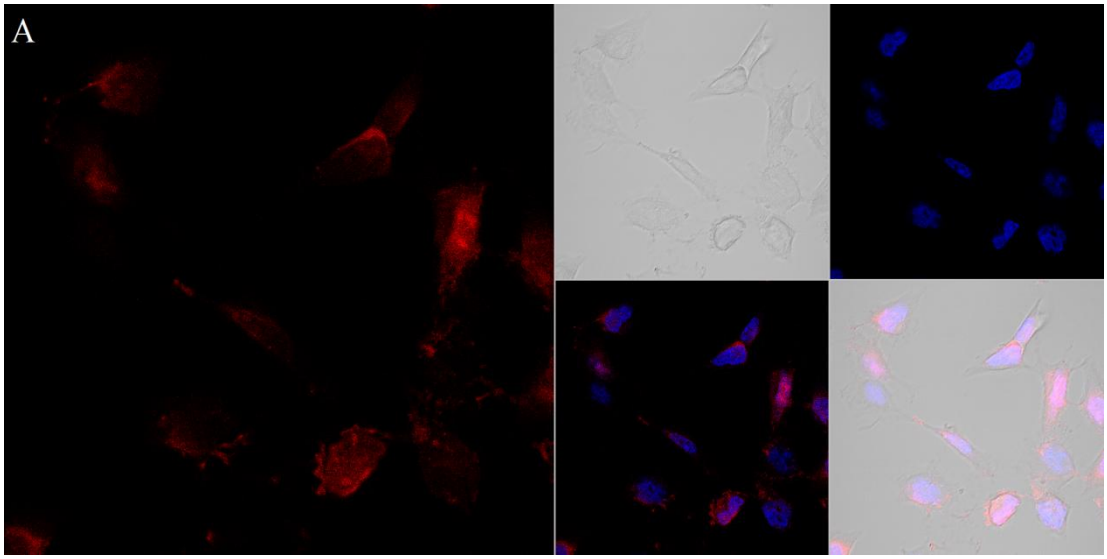

Figure 42. Confocal images of fixed HEK293 cells exposed to 50 μg/mL Au-MSA-PEG NCs for 24 hours prior to fixation. Clockwise from left: Au-MSA-PEG; bright field; DAPI; composite emissions from Au-MSA-PEG, DAPI, bright field; composite emissions of Au-MSA-PEG and DAPI. Images correspond to frame 10 of Figure 43 [reference 38– Reproduced by permission from The Royal Society of Chemistry].

Confirmation of NCs location inside the cells, rather than adsorbed onto the exterior of the cell membrane, z-stack imaging, as shown in Figure 43, confirmed Au-MSA-PEG NCs had made it past not only the cell membrane but also were located inside the nucleus. If this were not the case, and the NCs were making it into the cell but only adhering to the nucleus, then instead the z-stack would have shown red rings signifying adsorption of the NCs onto the membrane with no red signal inside the rings. Also of interest with regards to heterogeneous distribution was the difference between cells. Some cells had high concentrations of Au-MSA-PEG NCs in both the intracellular region and nucleus; some only high in the intracellular region and low in the nucleus; and some had high concentrations in the nucleus but low in the intracellular region.

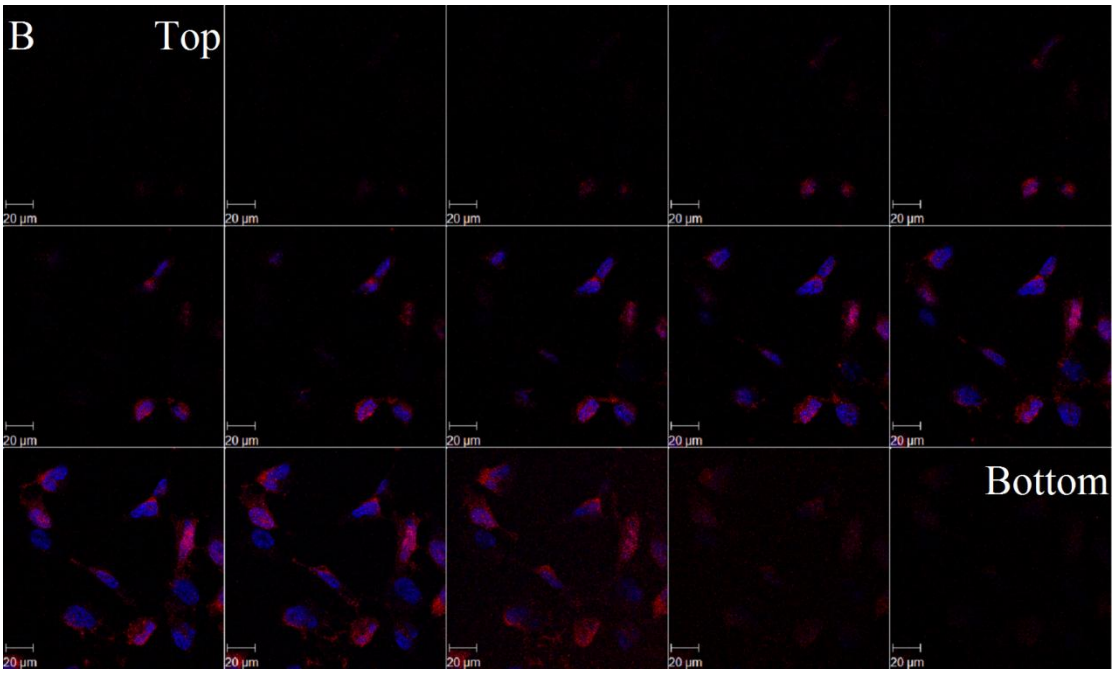

Figure 43. Confocal images of fixed HEK293 cells. The cells were exposed to 50 µg/mL Au-MSA-PEG NCs for 24 hours prior fixture. Z-stack images of composite emissions from DAPI and Au-MSA-PEG. The images were taken in a series of 15-step 1-µm-step-size measurements, starting from above the cell (TOP) toward the bottom of the cell [reference 38– Reproduced by permission from The Royal Society of Chemistry].

4.3 Dosage effect

Examination of effect of dosage on visibility of Au-MSA-PEG NCs was separately tested with both HeLa and HEK cells. Varied NCs concentrations over 1-50 µg/mL were tested with an incubation of one day. As can be seen in Figure 44, the lower concentrations provided limited visibility of the NCs. Au-MSA-PEG NCs were observed entering HeLa cells and the nucleus at the three higher concentrations. The NCs may have also entered the cells at lower concentrations, but at this sensitivity the signal was comparable with the control.

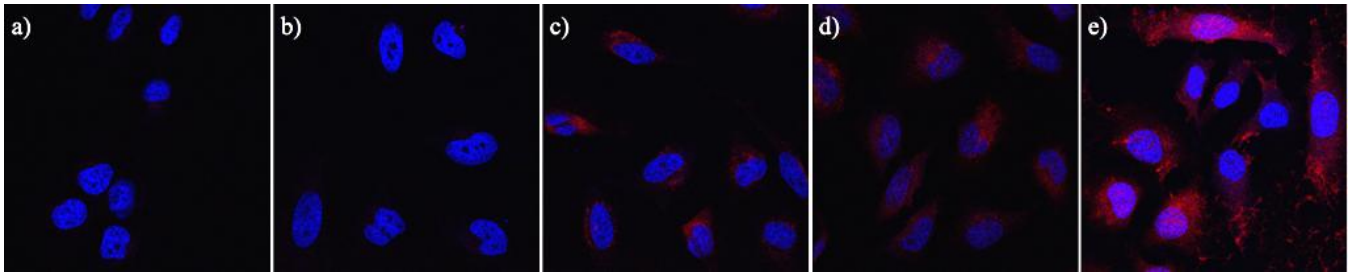

Figure 44. Confocal images of fixed HeLa cells. The cells were exposed to varied Au-MSA-PEG NCs concentrations for one day prior fixation. Blue is DAPI, red is Au-MSA-PEG. Brightness and contrast enhanced for illustration purposes. Panel A: 1 μg/mL, Panel B: 5 μg/mL, Panel C: 10 μg/mL, Panel D: 20 μg/mL, Panel E: 50 μg/mL.

As shown in Figure 45, similar results were observed with HEK cells. Much like occurred for HeLa cells, Au-MSA-PEG NCs entered both the cell and the nucleus. Both diffuse distributions and higher concentration clustering of the NCs were observed, again much as had been observed with HeLa cells. From the data for both HEK and HeLa cells it was determined 20 μg/mL would be a good concentration for additional experiments.

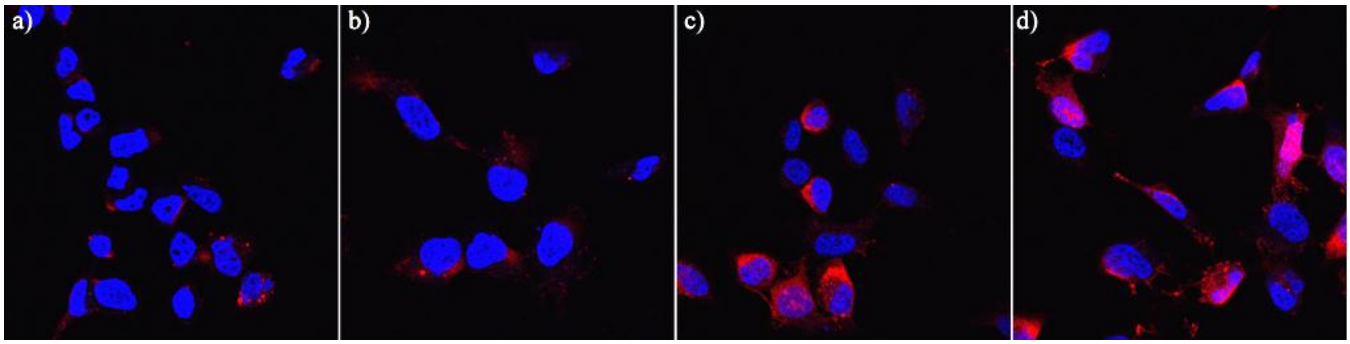

Figure 45. Confocal images of fixed HEK293 cells. The cells were exposed to varied Au-MSA-PEG NCs concentrations for one day prior fixation. Blue is DAPI, red is Au-MSA-PEG. Brightness and contrast enhanced for illustration purposes. Panel A: 5 μg/mL, Panel B: 10 μg/mL, Panel C: 20 μg/mL, Panel D: 50 μg/mL.

4.4 Duration effect

The duration of incubation, up to 24 hours, was examined to determine the amount of time necessary for sufficient penetration of Au-MSA-PEG NCs into the cells. In this case HEK cells were studied. As one would expect, longer durations led to more NCs accumulating inside the cells, as shown in Figure 46. The 24 hour duration provided the best results with the clearest

diffuse and heterogeneous distributions. From this data it was determined 24 hour incubations would be likely be the most beneficial for additional data collection.

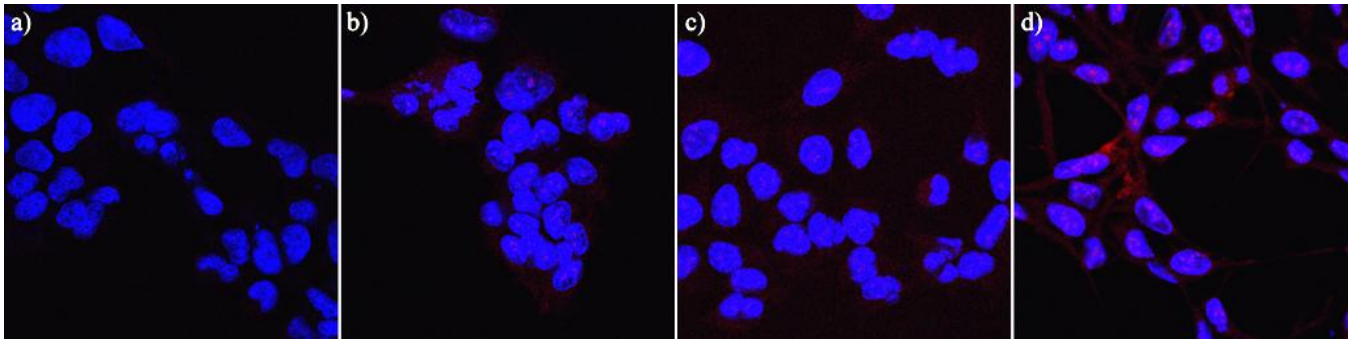

Figure 46. Confocal images of fixed HEK293 cells. The cells were exposed to 20 μg/mL Au-MSA-PEG NCs for varied durations prior fixation. Blue is DAPI, red is Au-MSA-PEG. Brightness and contrast enhanced for illustration purposes. Panel A: 3 hours, Panel B: 6 hours, Panel C: 18 hours, Panel D: 24 hours.

4.5 Cell life cycle

From the duration effect experiments it was noted Au-MSA-PEG luminescence did not always increase with duration. Also of note, in Figure 42 there were significant differences between cells for the accumulation of NCs in both the intracellular and nuclear regions. One would think that regardless of passive diffusion or active transport, greater durations of exposure would have led to stronger signal from the NCs. It was proposed that differences in the stages of the cell life cycle might have been playing a role in the internalization. This was tested by synchronizing HEK cells at the G1 phase prior to incubation. Upon removal of the inhibitor, the cells were incubated with Au-MSA-PEG at 20 μg/mL for up to 24 hours. As shown in Figure 47, continued though lessened variability in luminescence between cells, within a single time frame, and increasing and decreasing signal intensity as time increased, did not clarify whether or not the cell life cycle played a role in the appearance of bright clusters in the nucleus. Additional work in the future will be required to pinpoint what is leading to this very interesting phenomenon.

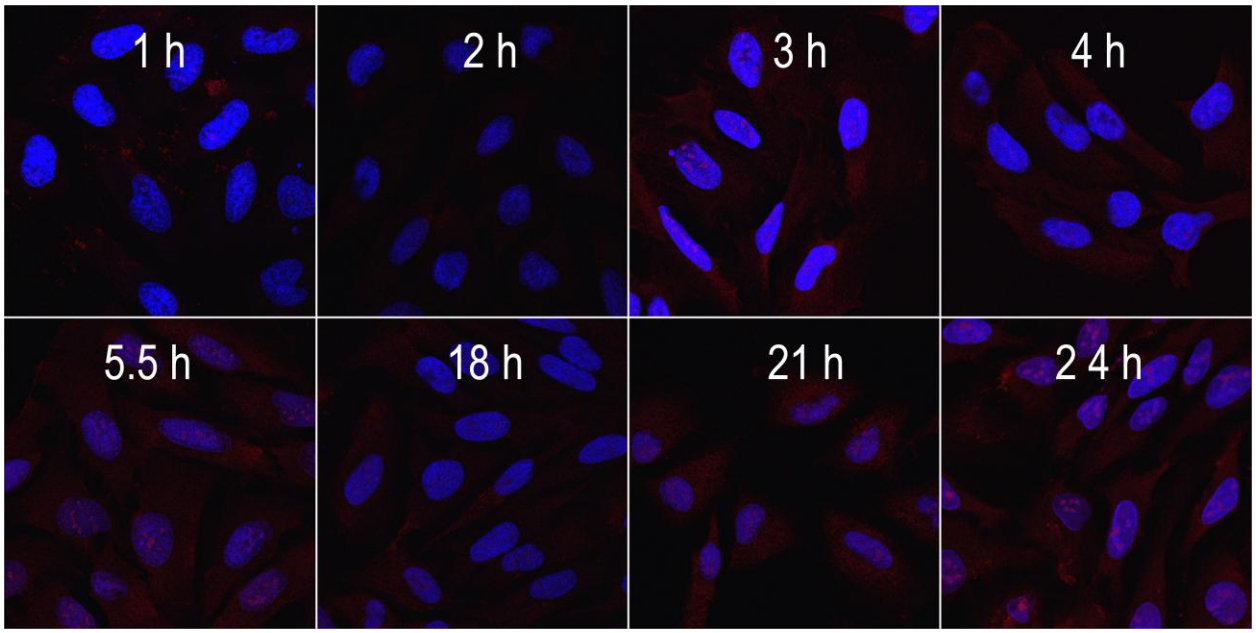

Figure 47. Fixed HeLa cells exposed to 20 μg/mL Au-MSA-PEG for varied durations prior fixture. Clustering of Au NCs in the nucleus by 24 hours has been observed in both HeLa and HEK cells. Brightness and contrast enhanced to better show Au-MSA-PEG accumulations.

4.6 Effect on offspring

The previously mentioned concern of cell toxicity also needed to be tested. A qualitative experiment to determine whether or not incubation for 24 hours would have a detrimental effect on the viability of HEK cells was set up. Much as was performed for the previous experiments, the cells were incubated with 20 μg/mL Au-MSA-PEG for 24 hours. Some of the cell wells were then processed for imaging, as previously described, while additional cell wells were washed in triplicate with PBS followed by the addition of new cell growth media. The latter set of cells were then incubated for an additional two days and then fixed in the same manner.

As shown in Figure 48, the previous observations of widespread and heterogeneous distributions of Au-MSA-PEG NCs were again noted. Those cells that were incubated for another two days had similar cell morphology and DAPI concentrations, but the signal from Au-MSA-PEG NCs was only a little above the control batch of cells. This qualitative examination agreed with some literature reports of the nontoxic nature of Au NCs.

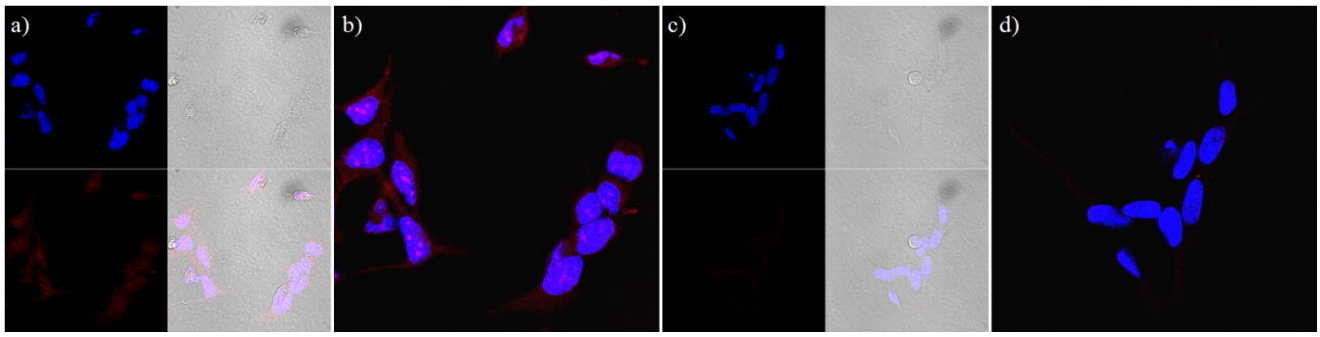

Figure 48. Confocal images of fixed HEK293 cells. The cells were exposed to 20 μg/mL Au-MSA-PEG NCs for 24 hours prior fixture. Panel A: clockwise from left: Au-MSA-PEG; Bright field; DAPI; Composite emissions from DAPI and Au-MSA-PEG; Composite image of bright field, DAPI and Au-MSA-PEG. These cells were fixed after exposure to Au-MSA-PEG. Panel B: HEK293 cells incubated in fresh cell growth media for 48 hours after washing away Au-MSA-PEG solution in which they had been incubated for 24 hours. Panel C: Brightness and contrast enhanced DAPI and Au-MSA-PEG overlay of Panel A. Panel D: Brightness and contrast enhanced DAPI and Au-MSA-PEG overlay of Panel B.

5 SUMMARY

In summary, heating monothiolate stabilized Au NCs for one day in the presence of excess like thiol significantly enhanced the near IR emission intensity. This was shown to be the case for two monothiolate Au NCs, MSA and tiopronin. It is proposed this approach may be generalizable to other small Au NCs on the scale of sub 2 nm core diameter. Enhancement of the luminescence intensity, approximately five times the initial QE, led to discernible signal when Au-MSA-PEG NCs were added to both HEK and HeLa cells for incubation.

Partially PEGlated Au-MSA-PEG NCs were observed to enter not only both cell types but also their nuclei. This observation adds to the body of literature showing NCs can enter the nucleus, but previous research on such typically involved use of a nuclear localization signal as part of the ligand. The appearance of clusters of accumulated Au-MSA-PEG inside the nucleus is quite interesting. The ability to further functionalize Au-MSA-PEG, with the low ratio of PEGlated ligands, makes it a promising probe for targeting both intracellular and nuclear pro-

cesses. Qualitative assessment of cell toxicity showed no noted cell morphology changes due to exposure to Au NCs.

The observed chemical stability and favorable optical properties of Au-LA NCs, along with the literature reports of their entry into cells, may provide a good base platform from which further attempts to modify the NCs, through coupling reactions, either for enhancement of QE or specific targeting. The resistance to thiol addition or exchange, retention of QE in cell growth media, and shorter wavelength, but still beyond 650 nm, makes for a potential probe that should be easy to detect with readily available near IR detectors.

6 REFERENCES

(1) Liu, J.; Yu, M.; Zhou, C.; Yang, S.; Ning, X.; Zheng, J., *J. Am. Chem. Soc.*, **2013**, *135*, 4978.
(2) Mooradian, A., Phys. Rev. Lett., **1969**, *22*, 185.
(3) Brust, M.; Walker, M.; Bethell, D.; Schiffrin, D. J.; Whyman, R., *J. Am. Chem. Soc., Chem. Commun.*, **1994**, *0*, 801.
(4) Jao, Y.-C.; Chen, M.-K.; Lin, S.-Y., *Chem. Commun.*, **2010**, *46*, 2626.
(5) Hu, M.; Chen, J.; Li, Z.-Y.; Au, L.; Hartland, G. V.; Li, X.; Marquez, M.; Xia, Y., *Chem. Soc. Rev.*, **2006**, *35*, 1084.
(6) Jin, R., *Nanoscale*, **2010**, *2*, 343.
(7) Murray, R. W. *Chem. Rev.*, **2008**, *108*, 2688.
(8) Link, S.; Beeby, A.; FitzGerald, S.; El-Sayed, M. A.; Schaaff, T. G.; Whetten, R. L., *J. Phys. Chem. B*, **2002**, *106*, 3410.
(9) Varnavski, O.; Ramakrishna, G.; Kim, J.; Lee, D.; Goodson, T., *J. Am. Chem. Soc.*, **2009**, *132*, 16.
(10) Ramakrishna, G.; Varnavski, O.; Kim, J.; Lee, D.; Goodson, T., *J. Am. Chem. Soc.*, **2008**, *130*, 5032.
(11) Zheng, J.; Zhang, C.; Dickson, R. M., *Phys. Rev. Lett.*, **2004**, *93*, 077402.
(12) Wang, G.; Huang, T.; Murray, R. W.; Menard, L.; Nuzzo, R. G., *J. Am. Chem. Soc.*, **2005**, *127*, 812.
(13) Wang, G.; Guo, R.; Kalyuzhny, G.; Choi, J.-P.; Murray, R. W., *J. Phys. Chem. B*, **2006**, *110*, 20282.
(14) Jadzinsky, P. D.; Calero, G.; Ackerson, C. J.; Bushnell, D. A.; Kornberg, R. D., *Science*, **2007**, *318*, 430.
(15) Heaven, M. W.; Dass, A.; White, P. S.; Holt, K. M.; Murray, R. W., *J. Am. Chem. Soc.*, **2008**, *130*, 3754.
(16) Zhu, M.; Eckenhoff, W. T.; Pintauer, T.; Jin, R., *J. Phys. Chem. C*, **2008**, *112*, 14221.

(17) Zhu, M.; Aikens, C. M.; Hollander, F. J.; Schatz, G. C.; Jin, R., *J. Am. Chem. Soc.*, **2008**, *130*, 5883.
(18) Wu, Z.; Gayathri, C.; Gil, R. R.; Jin, R., *J. Am. Chem. Soc.*, **2009**, *131*, 6535.
(19) Wu, Z.; Jin, R., *Nano Letters*, **2010**, *10*, 2568.
(20) Zheng, J.; Zhou, C.; Yu, M.; Liu, J., *Nanoscale*, **2012**, *4*, 4073.
(21) Duan, H.; Nie, S., *J. Am. Chem. Soc.*, **2007**, *129*, 2412.
(22) Habeeb Muhammed, M.; Ramesh, S.; Sinha, S.; Pal, S.; Pradeep, T., *Nano Res.*, **2008**, *1*, 333.
(23) Negishi, Y.; Nobusada, K.; Tsukuda, T., *J. Am. Chem. Soc.*, **2005**, *127*, 5261.
(24) Xie, J.; Zheng, Y.; Ying, J. Y., *J. Am. Chem. Soc.*, **2009**, *131*, 888.
(25) Devadas, M. S.; Kim, J.; Sinn, E.; Lee, D.; Goodson, T.; Ramakrishna, G., *J. Phys. Chem. C*, **2010**, *114*, 22417.
(26) Schaaff, T. G.; Whetten, R. L., *J. Phys. Chem. B*, **1999**, *103*, 9394.
(27) Lin, C.-A. J.; Yang, T.-Y.; Lee, C.-H.; Huang, S. H.; Sperling, R. A.; Zanella, M.; Li, J. K.; Shen, J.-L.; Wang, H.-H.; Yeh, H.-I.; Parak, W. J.; Chang, W. H., *ACS Nano*, **2009**, *3*, 395.
(28) Hicks, J. F.; Miles, D. T.; Murray, R. W., *J. Am. Chem. Soc.*, **2002**, *124*, 13322.
(29) Tang, Z.; Ahuja, T.; Wang, S.; Wang, G., *Nanoscale*, **2012**, *4*, 4119.
(30) Tang, Z.; Xu, B.; Wu, B.; Robinson, D. A.; Bokossa, N.; Wang, G., *Langmuir*, **2011**, *27*, 2989.
(31) Lin, S.-Y.; Chen, N.-T.; Sum, S.-P.; Lo, L.-W.; Yang, C.-S., *Chem. Commun.*, **2008**, 4762.
(32) Muhammed, M. A. H.; Verma, P. K.; Pal, S. K.; Kumar, R. C. A.; Paul, S.; Omkumar, R. V.; Pradeep, T., *Chem. - Eur. J.*, **2009**, *15*, 10110.
(33) Alkilany, A. M.; Lohse, S. E.; Murphy, C. J., *Acc. Chem. Res.*, **2012**, *46*, 650.
(34) Yang, L.; Shang, L.; Nienhaus, G. U., *Nanoscale*, **2013**, *5*, 1537.
(35) Shang, L.; Azadfar, N.; Stockmar, F.; Send, W.; Trouillet, V.; Bruns, M.; Gerthsen, D.; Nienhaus, G. U., *Small*, **2011**, *7*, 2614.
(36) Polavarapu, L.; Manna, M.; Xu, Q.-H., *Nanoscale*, **2011**, *3*, 429.
(37) Wang, H.-H.; Lin, C.-A. J.; Lee, C.-H.; Lin, Y.-C.; Tseng, Y.-M.; Hsieh, C.-L.; Chen, C.-H.; Tsai, C.-H.; Hsieh, C.-T.; Shen, J.-L.; Chan, W.-H.; Chang, W. H.; Yeh, H.-I., *ACS Nano*, **2011**, *5*, 4337.
(38) Conroy, C. V.; Jiang, J.; Zhang, C.; Ahuja, T.; Tang, Z.; Prickett, C. A.; Yang, J. J.; Wang, G., *Nanoscale*, **2014**, *6*, 7416.
(39) Kohlmann, O.; Steinmetz, W. E.; Mao, X. A.; Wuelfing, W. P.; Templeton, A. C.; Murray, R. W.; Johnson, C. S., *J. Phys. Chem. B*, **2001**, *105*, 8801.
(40) Jiang, J.; Conroy, C. V.; Kvetny, M. M.; Lake, G. J.; Padelford, J. W.; Ahuja, T.; Wang, G., *J. Phys. Chem. C*, **2014**, *Submitted*.
(41) Zhan, N.; Palui, G.; Grise, H.; Tang, H.; Alabugin, I.; Mattoussi, H., *ACS Appl. Mater. Interfaces*, **2013**, *5*, 2861.
(42) Zhou, C.; Long, M.; Qin, Y. P.; Sun, X. K.; Zheng, J., *Angew. Chem., Int. Ed.*, **2011**, *50*, 3168.
(43) Sahyun, M. R. V.; Serpone, N., *J. Phys. Chem. A*, **1997**, *101*, 9877.
(44) Templeton, A. C.; Chen, S.; Gross, S. M.; Murray, R. W., *Langmuir*, **1999**, *15*, 66.

7 APPENDICES

A Chemicals

Tetrachloroauric acid trihydrate ($HAuCl_4 \cdot 3H_2O$, >99.99%), mercaptosuccinic acid (MSA, 97%), N-(2-mercaptopropionyl)glycine (tiopronin, ≥98.0%), sodium borohydride ($NaBH_4$, 99%), deuterium oxide (D_2O, 99.9%), acetic acid (CH_3COOH, 99.7%) methanol (CH_3OH, 99.8%), tris(hydroxymethyl)aminomethane (THAM, ≥99.8%), methoxypolyethylene glycol amine (PEG, 750), N-(3-dimethylaminopropyl)-*N'*-ethylcarbodiimide hydrochloride (EDC, ≥99.0%), 3,3'-diethylthiatricarbocyanine iodide (DTTC, 99%), were purchased from Sigma-Aldrich and used as received. Potassium phosphate monobasic (KH_2PO_4, ≥99.5%) and potassium phosphate dibasic (K_2HPO_4, ≥99.0%) were purchased from Fluka and used as received. Nucleus stain dye 4',6-diamidino-2-phenylindole (DAPI) was used as received.

B Measurements

A Shimadzu UV-1700 spectrophotometer was used to measure UV-visible absorbance (UV-vis). Fluorescence spectra were recorded with a Horiba Jobin-Yvon Fluorolog 311 spectrometer equipped with PMT visible and InGaAs near IR detectors. A Hoya Y-44 long-pass filter was used to collect emission spectra. QE was calculated from the combined detector responses with the corresponding absorbance values ranging 0.08-0.15 at the wavelength of excitation (400 nm). DTTC in methanol was used as standard (QE=21%).[43] NMR spectra were collected with a Bruker NMR 400 MHz spectrometer. Confocal imaging was performed using a Zeiss 510 Laser Scanning Microscope with a 405 nm laser and a 600 nm long-pass filter.

C Synthesis of Au-MSA, Au-Tio NCs

A modified one-phase Brust-Schiffrin synthesis was employed for both Au-MSA and Au-Tio nanoclusters (NCs).[44] In a representative synthesis, $HAuCl_4 \cdot 3H_2O$ was mixed with a certain

equivalence of MSA in 20 mL solvent, 6:1 methanol: acetic acid, and stirred until solution turned colorless. The solution was then placed in an ice bath. After the temperature equilibrates, twenty equivalents of freshly prepared $NaBH_4$ in 10 mL chilled nanopure water were quickly added under rapid stirring. The addition of reductant was energetic and associated with extensive gas formation, necessitating care to avoid spill. The solution immediately turned dark. Solvent was removed by rotary evaporator after rapid stirring for three hours. The final products were purified by three days of dialysis using snakeskin pleated dialysis tubing (Thermo Scientific, 3500 MWCO).

D Thermo treatment of Au-MSA, Au-Tio NCs

Additional thiols at designed equivalents relative to the ligands on Au nanoclusters were added to a solution of Au nanoclusters in nanopure water. The solution was stirred at moderate speed at elevated temperature (mostly 50 °C) in an oil bath for 24-hours. Afterward, purification by dialysis was performed. The number of attached ligand was estimated based upon dried nanocluster mass and the previous assumed composition of $Au_{25}MSA_{18}$ and the literature composition of $Au_{201}Tiopronin_{85}$ respectively. Note the uncertainty induced by the estimation of different nanocluster compositions is insignificant for the thiol:ligand ratio adopted in the etching process.

E PEGylation of Au-MSA, Au-Tio NCs

In a representative coupling reaction, the etched Au nanoclusters ($1.9x10^{-7}$ moles) were mixed with ca. five equivalents PEG750 (0.72 mg) and fifty equivalents EDC (1.8 mg) in 10 mL nanopure water at pH 8. The solution was stirred at room temperature overnight. The products were purified by dialysis. The coupling efficiency, mole ratio of PEGlated versus total ligands, was determined by ^1H NMR. Each PEG750 was estimated to have 15 (CH_2CH_2O) units, or 60

protons at 3.6 ppm. The CH_2 of MSA at 3.1 ppm and the CH_3 of tiopronin at1.6 ppm were used to calculate the peak intensity and thus PEG:thiolate ratio.

F Coupling PEG, rhamnose to Au-LA NCs

The coupling reaction proceeded the same as for coupling PEG to Au-MSA or Au-Tio NCs. Coupling efficiency was determined by integrating over 1.0-2.5 ppm, which corresponded ten hydrogen atoms on C2-C5 plus C7 from lipoic acid. When analyzing PEG, the previously mentioned 60 hydrogen atoms at 3.6 ppm were integrated and compared. When analyzing for the rhamnose derivative, the 2.5-4.1 ppm range was integrated. This span encompassed nine hydrogen atoms from rhamnose, based on ^{1}H NMR of free rhamnose derivative, and three hydrogen atoms from C6 and C8 of lipoic acid.